BOSTON UNIVERSITY
COLLEGE OF ENGINEERING

Thesis

CHARACTERIZATION OF THE IMAGING ELECTRON SPECTROMETER

by

Slavik Braginsky

B.S., Boston University, 1995

Submitted in partial fulfillment of the requirements
for the degree of

Master of Science

Boston University, College of Engineering

1997

Approved by

First Reader _____ 4/9/97
Prof. Theodore Fritz — Date

Second Reader _____ 4/10/97
Prof. William Oliver — Date

Third Reader (Chair) _____ 4/9/97
Prof. Krish Chakrabarty — Date

Boston University
1997

Dedicated to my parents
Yan and Emilya, and my brother Alex.

ACKNOWLEDGMENTS

Recognition is made to the entire Energetic Particle Group at Boston University, Center for Space Physics. Their effort in supporting instrument testing and analysis has produced a high level of understanding of the instrument functionality. Also, their input into my thesis defense presentation greatly enhanced my presentation to become more clear and comprehensive.

Specifically, appreciation is extended to Dr. Rob Sheldon and Dr. David Matthews who were integrally involved in the testing and analysis of the IES calibrations. Their effort in traveling for test support and analysis of instrument performance had contributed many long hours, and produced comprehensive results to bestow a wealth of critical information of the instrument. Also, appreciation is given to Mr. Mohamed Alothman for contributing his scientific knowledge toward my understanding of the IES, and aid toward the publication of this thesis during his own busy schedule.

I'd like to thank all my committee members (Prof. Theodore Fritz, Prof. William Oliver, and Prof. Krish Chakrabarty) for their insight into how to better correspond the information of this thesis. This document has undergone many revisions to better portray how this instrument has become a comprehensive tool, and this was by no small means contributed by my readers and chair while accompanying their busy schedule.

Lastly, I'd like to take the opportunity to thank Prof. Fritz. Prof. Fritz has been involved in every aspect of the analysis of the IES, and has dedicated more time than

anyone I can imagine toward this instrument. He has guided the testing as well as the analysis, and always showed support for all aspects of the IES work I had been involved with. Prof. Fritz has always shown trust in my abilities by including me in the efforts associated with the programs he is involved with, and I am grateful to have been given these opportunities. Throughout the years it has always been a true learning experience which I consider invaluable, and am honored to have had the chance to experience working with him. Thank you.

CHARACTERIZATION OF THE IMAGING
ELECTRON SPECTROMETER

(Order No.)

Slavik Braginsky

Boston University, College of Engineering, 1997

Major Professor: Prof. Theodore A. Fritz
Prof. of Astronomy
Prof. of Electrical & Computer Engineering

Abstract

The Imaging Electron Spectrometer (IES) represents a compact, light-weight spacecraft instrument capable of high resolution energetic particle measurements. Seven IES units have been fabricated as part of scientific payload aboard satellite and rocket missions. The IES has exhibited a number of dependencies on its operational mode and environment. The instrument has demonstrated a baseline fluctuation as a function of temperature, time constant of operation, and incident particle intensity resulting in difficulties obtaining reliable and comprehensive measurements. In order to parameterize these dependencies, I have supported extensive calibrations at NASA/Goddard Space Flight Center and investigated thermal dependencies provided by Los Alamos National Laboratory's. As part of my research, I have analyzed these calibrations and related them to instrument performance. The results of these calibrations are provided, and the concept

behind the instrument's operational modes and electronic background is reviewed to better understand the IES response to its environment and mode of operation. These results are specifically applicable to characterizing IES#6, but the general concepts are applicable to all IES instruments.[1]

[1] This effort has been supported within the Center for Space Physics at Boston University by NASA Grant NAG5-2266.

TABLE OF CONTENTS

LIST OF FIGURES

Number *Page*

LIST OF TABLES

GLOSSARY

ADC	Analog-to-Digital Converter
BU	Boston University
CEPPAD	Comprehensive Energetic Particle Pitch Angle Distribution
CME	Coronal Mass Ejection
DPU	Data Processing Unit
EHP	Electron Hole Pair
FWHM	Full Width at Half Maximum
Gd-153	Gadolinium 153.
GGS	Global Geospace Science
GSFC	Goddard Space Flight Center
HIST	High Sensitivity Telescope
IDA	Inst. F. Datenverarb. Anlagen
IES	Imaging Electron Spectrometer
IIMS	Imaging Ion Mass Spectrometer
IPS	Imaging Proton Spectrometer
IST	Integrated Systems Test
ISTP	International Solar Terrestrial Physics
LANL	Los Alamos National Laboratory
LUT	Look-Up Table
MPAe	Max Planck Institute for Aeronomy
MXRP	Microplex RAPID
RAL	Rutherford Appleton Laboratory
RAPID	Research with Adaptive Particle Imaging Detectors
PULSAUR	Pulsating Aurora

Chapter 1

IES Instrument Overview

1.1 IES Instrument Configuration

The Imaging Electron Spectrometer consists of three sets of three-element ion-implanted Si detectors situated beneath a pinhole aperture. Figure 1.1a illustrates one of the three IES sensor head segments containing three Si detection elements with the corresponding shielding. Although the aperture above the elements allows a 100° field of view, the Si elements are positioned behind the pinhole to provide a field of view of 20° per element, as is illustrated in figure 1.1b. Therefore, with nine elements the collective IES field of view is 180°. This allows the IES to correlate its measurements of energetic particles with a trajectory denoted by the Si element used to detect it. The IES sensor head with an exploded view of a segment such as the one depicted in figure 1.1a is illustrated in figure 1.2.

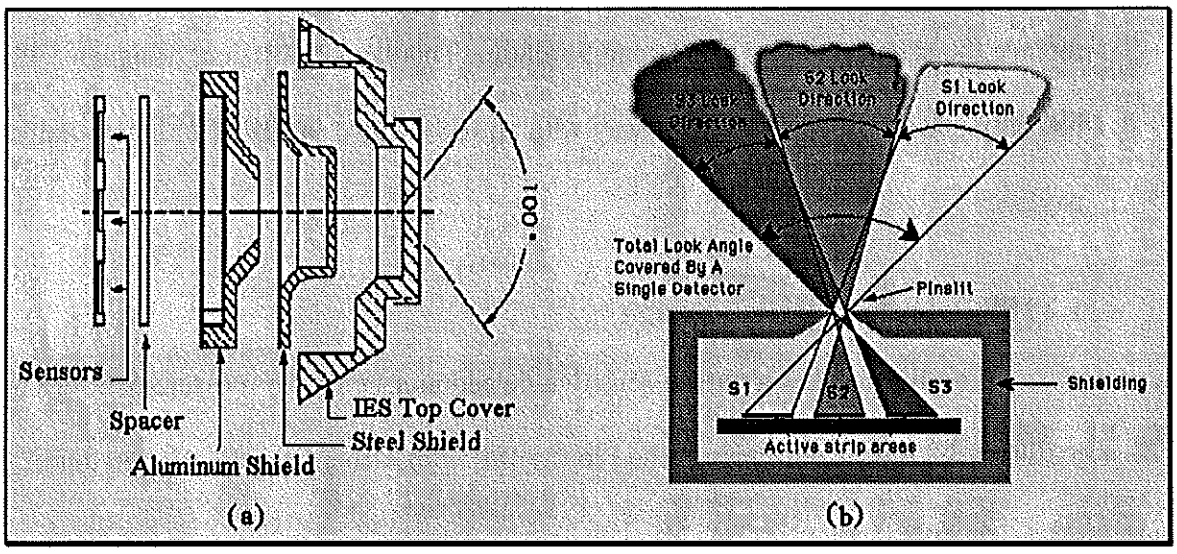

Figure 1.1: (a) IES sensor and shielding configuration. (b) IES angular detection scheme.

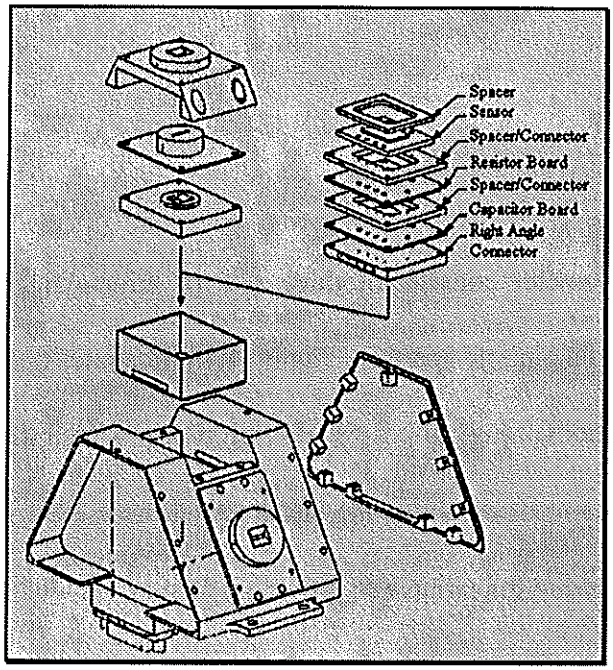

Figure 1.2: IES sensor head configuration.

The first IES launched, IES# 3, was part of scientific payload on a sounding rocket mission designated Pulsaur II, where a number of instrument response difficulties were initially recognized. An IES modified with six additional, small element, solid state detectors was successfully launched on the Polar spacecraft on February 24, 1996. It is also part of the Cluster launch mission where four satellites, each containing an IES, IES# 1, 2, 4, & 5, were launched out of Kourou, French Guiana. Cluster was launched on June 4, 1996, but due to system errors, the Ariane-5 rocket transporting the satellites into orbit was self-detonated as a result of veering off course. As a result a new Cluster launch mission was instituted to replace the science lost by the Ariane-5 failure. This launch mission, designated Phoenix, has only one satellite and is under way with an IES instrument (IES# 6) incorporated on its payload.

1.2 IES Particle Detection Design

The IES utilizes a charge-sensitive detection scheme for measurement of energetic particles. Si diodes are implemented in the IES with a characteristic conversion of 3.6 eV

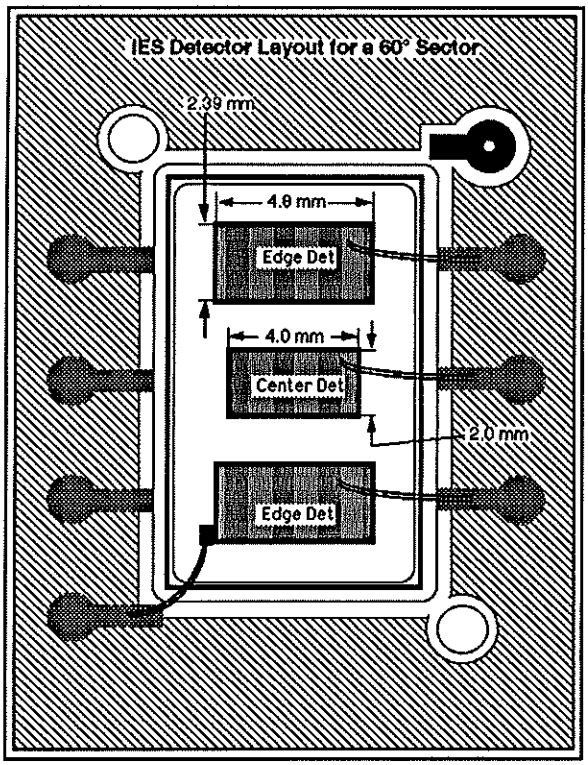

Figure 1.3: IES sensor board layout.

per electron hole pair (EHP) generated. This relationship between the energy of radiation deposited within a solid state device and the number of charge carriers produced by this interaction makes semiconductor diodes ideal for energetic particle measurement. Figure 1.3 depicts the sensor board outside the configuration illustrated in figure 1.2. Three Si elements are incorporated into one board such that a smaller Si element is in the center directly beneath the pinhole aperture with two identical, larger elements mirrored on the sides of the center element. In order to filter protons and photons from corrupting the charged particle measurements, a 152 μinch thick (1.39 g/cm^3) aluminized mylar foil is positioned in front of the Si detectors (Personal Communication: Prof. Theodore Fritz, BU). Figure 1.4 illustrates the instruments response to protons from the calibrations performed at Goddard Space Flight Center.

The electronic support provided for the Si detectors is an integrated circuit chip (MXRP) developed at the Rutherford Appleton Laboratory (RAL) in the United Kingdom. The MXRP features 16 channels of operation; only 9 channels are utilized for the IES. Each channel is supported by a charge sensitive preamplifier for 1st stage amplification of

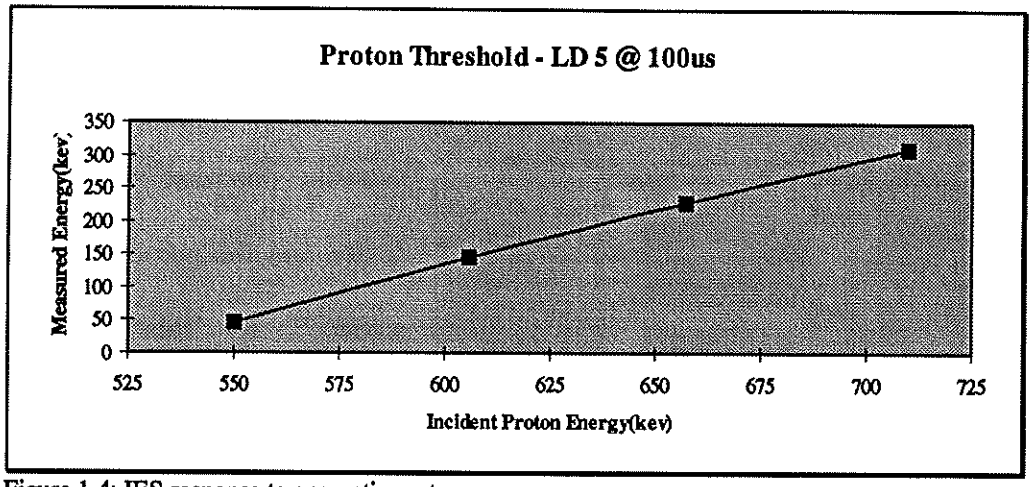

Figure 1.4: IES response to energetic protons

the detected signal and follow-on digitization electronics. The electronics supporting the MXRP has been designed with the capability for operating with four possible accumulation time settings predetermined to be 2 μs, 10 μs, 50 μs, or 100 μs. The implications of these time constants on instrument performance will be discussed later.

Each of the 16 channels of the MXRP has associated with it a voltage offset which defines the baseline for that particular channel. This voltage offset is designated as a "Pedestal", and any signal accumulated by the instrument will be added to this pedestal to produce an output voltage equal to the sum of the pedestal and signal voltages. However, the pedestal varies from channel to channel and has dependencies upon the time constant of operation, the temperature of the environment, and the incident particle beam intensity. Calibration of the MXRP response to variations in these dependencies is critical to understanding the data returned by the IES, and is supplied here.

1.3 MXRP System Design

The MXRP is an integrated chip developed at RAL with support for 16 data channels. Figure 1.5 illustrates one channel along with a timing schematic. An electron incident on the solid state device induces a small current to conduct through it by generating EHP's at a rate of 1 EHP per 3.6 eV deposited. This conductive current i produces a voltage drop at node *V1* from 300 V to $300\ V - (2\ M\Omega \bullet i)$. This charge coupled across the 470 pF capacitor is $Q=C(i \bullet R)$, where R is the 2 MΩ resistor, i is the current induced by the energetic particle interaction with the Si element, and C is the 470 pF capacitor. In order to maintain the virtual ground at the pre-amp input, a voltage is induced at the pre-amp output equivalent to Q, calculated above, divided by the 0.2 pF feedback capacitor. Combining terms yields:

$$V_{out} = (470\ pF \bullet i \bullet R)/(0.2\ pF) = 2350 \bullet i \bullet R.$$

Charge is then accumulated on the C1 and C2 capacitors by enabling the S1 and S2 inverted switches. When S1 and S2 go low, background signal is accumulated in C1 and C2. S1 is then set high to disable C1 from accumulating charge during signal integration, as C2 continues to integrate. S2 is then set high once integration is completed to disable C2. The signal is determined to be the charge accrued in C2 less the charge accrued in C1. The two capacitors are discharged at the appropriate time onto the data lines through enabling switches S3 and S4.

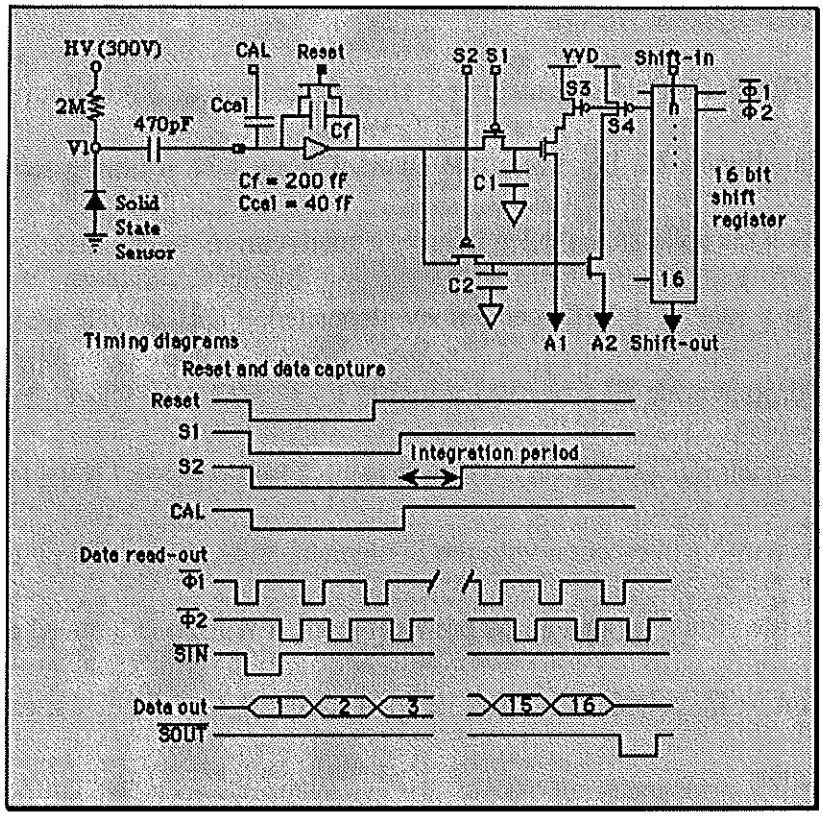

Figure 15: MXRP schematic and timing diagram.

1.4 Geometric Factor

The counting rate of the IES is dependent upon the geometrical dimensions of the pinhole aperture with respect to the solid state devices used to detect the energetic particles, as well as the dimensions of the solid state devices. Assuming an isotropic intensity, the IES counting rate is $C_R = GI_o$, where G is the geometric factor of the IES, I_o is the isotropic particle intensity, and C_R is the IES-measured counting rate. Thus, calculating the IES-measured counting rate and the instrument's geometric factor, the isotropic particle intensity of the instrument's environment can be calculated. Figure 1.6 depicts the incremental

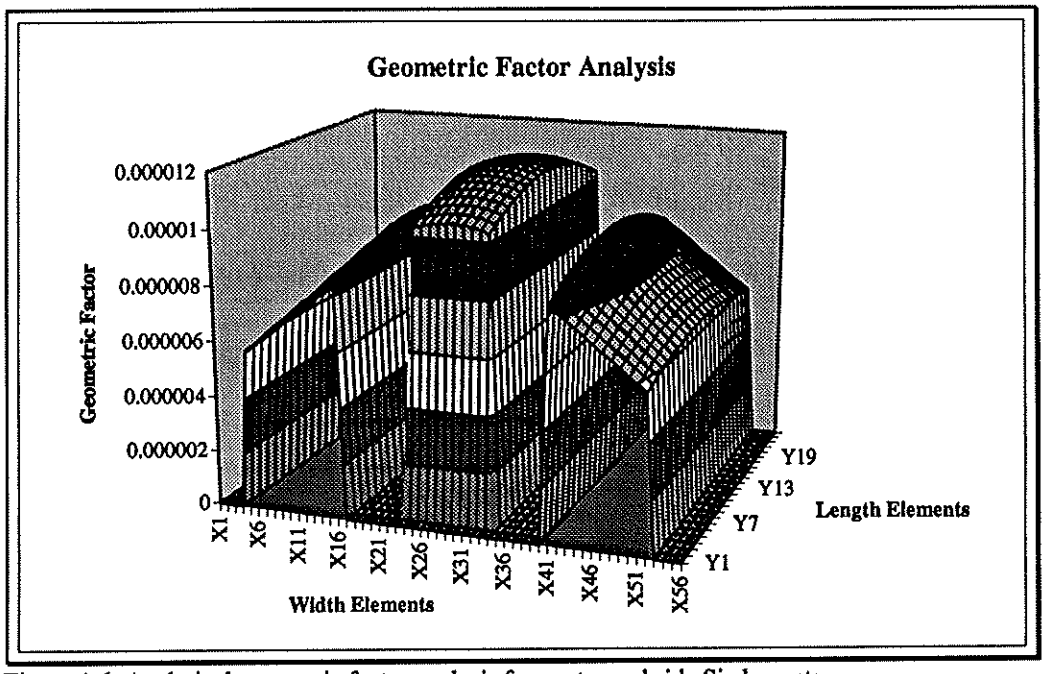

Figure 1.6: Analytical geometric factor analysis for center and side Si elements.

geometric factors for the center and side elements of one head segment (only one depicted due to symmetry). The geometric factor for this sensor is derived by integrating the expression $\iint \frac{(A_1 A_2)\cos^2(\theta)}{r^2} d\Omega$ (Sullivan, 1971). Where A_1 represents the area of the detecting Si element, A_2 represents the area of the aperture, θ represents the angle between the incident particle path and the normal to the detecting plane, r represents the radial distance of the particle path between the two defining aperture areas, and $d\Omega$ represents the element of the solid angle. The result yields a geometric factor of 0.002228 $cm^2 \bullet ster$ for the center element, and 0.002195 $cm^2 \bullet ster$ for each side element.

1.5 Data Handling

The MXRP chip produces a voltage signal which is proportional to the energy deposited from the energetic particle. This signal is then amplified and digitized for data handling. An 8-bit analog-to-digital converter (ADC) is utilized such that, in combination with the differential amplifier, an 8-bit digital signal is assigned to a given energy range where the ADC gives full-scale (i.e. Energy bin 2^8=256) for an input signal of approximately 60 mV. The control logic assigns a 4-bit directional value to associate the energy bin with the correct detecting element. The corresponding 12 bits serve as an input vector for a bin definition look-up table (LUT) that provides an 8-bit address for the appropriate counter to increment (i.e., increment the number of times a particular energy

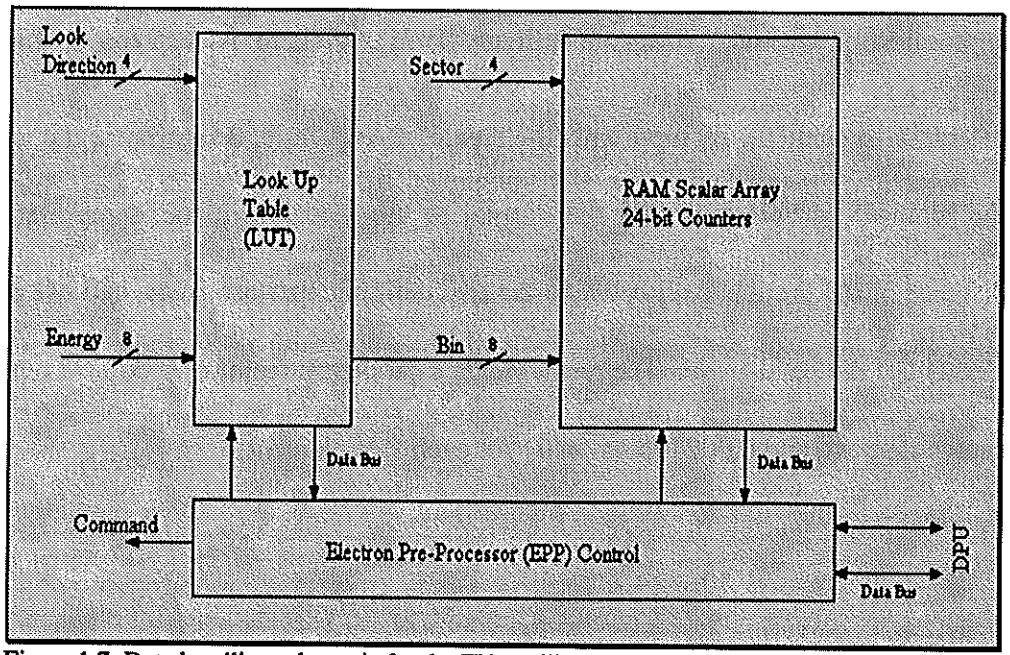

Figure 1.7: Data handling schematic for the IES (Wilken, 1997).

was recorded by a particular element). A 4-bit sector value is also generated to denote where in space the instrument is directed. The appropriate counter to increment is then selected by the 4-bit sector parameter and the 8-bit address generated from the LUT. Figure 1.7 illustrates this process.

Chapter 2

IES Operational Overview

2.1 Operational Modes

The IES utilizes an 8-bit ADC to assign 256 possible energy bins, ranging from bin 0 to 255, for particle detection. An incident particle with a defined energy will be converted into an 8-bit digital signal based on its analog voltage produced by the MXRP chip. The energy gain for the system has been measured to yield approximately 2.0 kev/channel. This produces an energy scale ranging up to 2.0 keV/channel • 256 channels = 512 keV. Therefore, ideally an energetic particle with an energy between 510 keV to 512 keV will be assigned a value of 255 by the ADC. However, the IES has been designed such that a particle with energy greater than the upper scale range will simply be assigned 255 by the ADC as well. This operational mode is defined as histogram mode, and table 2.1 illustrates the sorting of particles through the IES system with P denoting the channel number position of the pedestal, included in order to adjust for the baseline offset mentioned earlier.

Energy ADC Channel	Energy Lower Limit (kev)	Energy Upper Limit (kev)
0	0 - 2P	2 - 2P
1	2 - 2P	4 - 2P
.	.	.
.	.	.
.	.	.
254	508 - 2P	510 - 2P
255	510 - 2P	Above 510 - 2P

Table 2.1: IES histogram bin definition.

The IES will operate in 16-bin mode for most of its operation due to telemetry bandwidth limitations. The 256 energy bins are compressed into 16 energy bins through pedestal relations. Table 2.2 denotes how this conversion is done given the pedestal centroid position, P, the full width at half maximum, FWHM, of the pedestal gaussian distribution (S), and eight boundary offsets, B1 to B8, out of the 256 . The default values for the selected boundaries B1 to B8 are provided in table 2.3, and are subject to possible

Data Acquisition: Mapping of ADC-Channels to Bins		Assignment of Bins to Energy Intervals		
E-ADC Channel range Range: 0...255	Bin Number Range: 0...15	E-3DD(BM) Range: 0...11	E-3DD(NM) Range: 0...7	E-PAD Range:0...1
0	0			
1...(P-2S-1)	1			
(P-2S)...(P-S-1)	2	0		
(P-S)...(P-1)	3	1	0	
P...(P+S-1)	4	2	1	
(P+S)...(P+2S-1)	5	3		
(P+2S)...(P+B1-1)	6	4	2	0
(P+B1)...(P+B2-1)	7	5	3	0
(P+B2)...(P+B3-1)	8	6	4	0
(P+B3)...(P+B4-1)	9	7	5	0
(P+B4)...(P+B5-1)	10	8	6	1
(P+B5)...(P+B6-1)	11	9	6	1
(P+B6)...(P+B7-1)	12	10	7	1
(P+B7)...(P+B8-1)	13	11	7	1
(P+B8)...254	14			
255	15			

Table 2.2: IES data conversion table from histogram mode to 16-bin mode (As of 01/28/97) (Personal Communication: Mr. Rainer Rathje, IDA).

B1	B2	B3	B4	B5	B6	B7	B8
21	29	41	56	78	109	151	210

Table 2.3: Default boundary values for histogram mode compression (Personal Communication: Mr. Rainer Rathje, IDA).

modification prior to the launch of IES #6. The selection of these boundaries will be discussed later in regards to the baseline fluctuations with particle intensity.

2.2 Integration Time Constant

The IES has the ability to accumulate sensor data before data processing for four different integration times as mentioned earlier, i.e., 2μs, 10μs, 50μs, 100μs. This has been incorporated in the design in order to allow for reliable operation in environments with various particle intensity profiles. Pile-up is an effect recorded when during an accumulation period, i.e., integrated time constant, more than one particle interacts with the system. This has the effect of producing a data signal equivalent to the sum of the particles' energies. This effect can be reduced by operating the instrument with a shorter accumulation time per data sample. During periods of high particle intensity it is desirable for the instrument to be in a mode with a smaller active time of accumulation per data sample. This is incorporated into the system design in order to overcome problems of pile-up and baseline fluctuations, which will be covered in later chapters.

For each accumulation period there is a fixed period of time to cycle through each of the detector outputs for transcribing the accumulated channel response. This fixed period becomes a "dead time" during which no further data accumulation can occur. The IES dead time has been determined during the unit's calibration to be 48 μs. Knowing this parameter, the percent live time (percent of time the instrument is accumulating data per an accumulation and processing cycle) can be determined by:

$$\text{Live Time}(\%) = \left(\frac{\textit{Integration Time}}{\textit{Integration Time + Dead Time}}\right)\times 100$$

The percent live time for the IES is 4.00%, 17.24%, 51.02%, and 67.57% for the 2μs, 10μs, 50μs, and 100μs integration time constants, respectively. Thus during instances of high particle intensity, a lower time constant should be selected.

Figure 2.1 illustrates pile-up during calibration tests performed at Goddard Space Flight Center. The top panel illustrates the pedestal centered at channel 28, a response due to a beam of 100 keV electrons centered at channel 75, and a modest pulse pile-up centered at channel 121. The pile-up pulse is the result of two 100 kev electrons interacting with the IES during one integration cycle. This is easily determined by determining that the energy of the pile-up pulse is twice that of the 100 kev pulse. Thus, the number of channels between pile-up and pedestal is twice that of the 100 kev pulse and pedestal. The lower panel illustrates the result if intensity is increased, with increased instances of pile-up resulting in the observed histogram.

The IES time constant utilized is determined by ground command or through an autoswitching algorithm. For a given period of time per satellite rotation, or spin cycle, the total count rate, T, for pedestal and signal is summed and compared with a summed signal count rate, S. When $S \geq \frac{T}{H}$ for the default high flux ratio, H of 8, a shorter integration time is selected to compensate for the high intensity particle environment by the on-board software in the data processing unit (DPU). A longer integration time is selected to

compensate for the low intensity particle environment if $S \leq \frac{T}{L}$ for the default low flux ratio, L of 64.

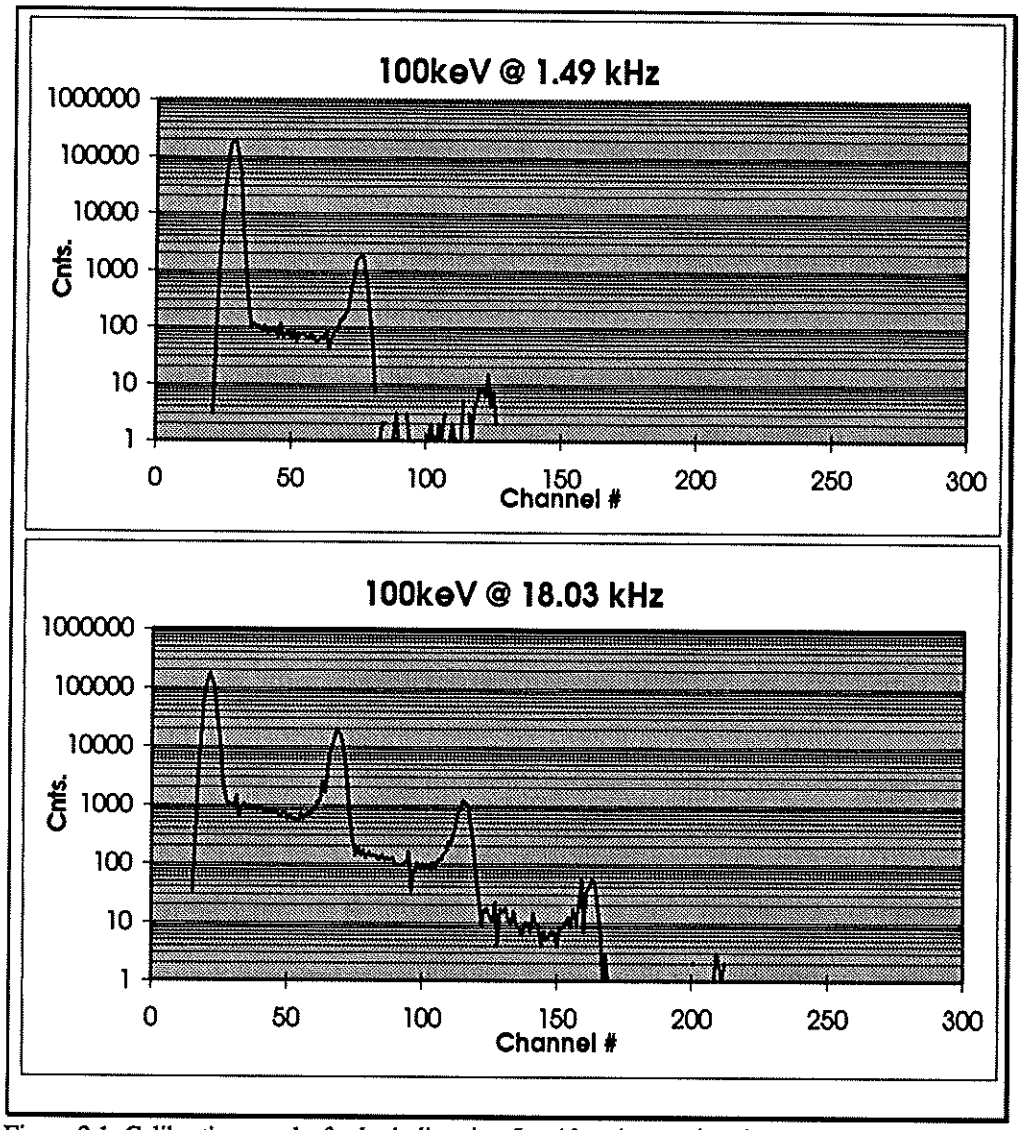

Figure 2.1: Calibration graphs for look direction 5 at 10 μs integration time. Data was taken with 100 keV electrons at intensities of 1.49 kHz and 18.03 kHz.

2.3 Sectored Data Format

Each look direction for the IES is sectored over a given spin period to provide the 3-dimensional realization of the spatial particle environment. Table 2.4 provides the organization of the 96 sectors which the IES senses for the Cluster and Phoenix satellites. Look directions 1, 2, 3, 7, 8 , and 9 have half the sector resolution of look directions 3, 4, and 5. This has been organized to redistribute the instrument memory resources for higher resolution of energy measurements.

ID	Sector															
	0	1	2	3	4	5	6	7	8	9	10	11	12	13	14	15
1	0		1		2		3		4		5		6		7	
2	8		9		10		11		12		13		14		15	
3	16		17		18		19		20		21		22		23	
4	24	25	26	27	28	29	30	31	32	33	34	35	36	37	38	39
5	40	41	42	43	44	45	46	47	48	49	50	51	52	53	54	55
6	56	57	58	59	60	61	62	63	64	65	66	67	68	69	70	71
7	72		73		74		75		76		77		78		79	
8	80		81		82		83		84		85		86		87	
9	88		89		90		91		92		93		94		95	

Table 2.4: Sectorization of spatial look directions for the IES (Personal Communication: Mr. Rainer Rathje, IDA).

2.4 Operational Look-Up Table

The pedestal of the IES has been defined as the baseline for each channel of the instrument energy response with respect to the detection of particles. This baseline voltage has dependencies on the integrated time constant of operation, instrument temperature, particle intensity profile, and is also distinctive to the detection element (look direction or electronics channel). It is necessary to determine the position of the pedestal with respect to

all dependencies in order to accurately sort the data into the appropriate energy bins given in tables 2.2 & 2.3. Based on the calibrations performed on the IES, three parameter look-up tables have been created to trace the pedestal position fluctuations based on information concerning look direction, time constant, and temperature of operation. These variations are discussed in Chapter 3.

Chapter 3

IES Operational Dependencies

3.1 IES Temperature Dependency

The IES instrument has exhibited a dependency of its energetic particle measurements on the temperature of the instrument's operation. This has been analyzed through the dependency of the pedestal to this effect. As temperature is increased, the pedestal exhibits a shift to higher histogram channels. This corresponds to the energy baseline shifting to a higher voltage offset. Also, the noise of the system, analyzed through FWHM measurements, increases with temperature. Figure 3.1 illustrates the pedestal position as a function of the operational time constant and temperature for look direction 1. Table 3.1 conveys the calibration data taken at Los Alamos on September 24, 1996 of the pedestal position as a function of time constant, temperature, and look direction for IES# 6.

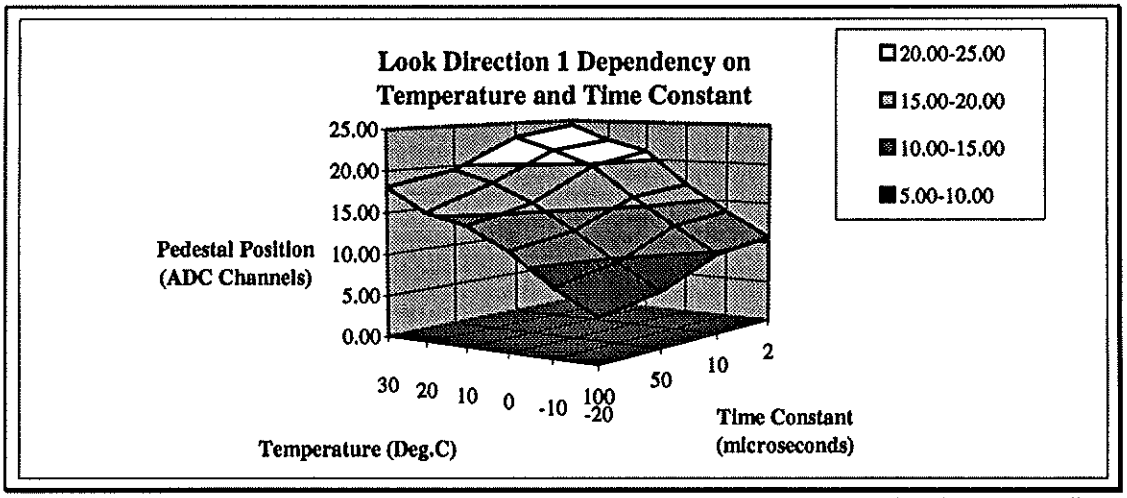

Figure 3.1: Temperature and time constant dependency of pedestal position for look direction 1 of IES# 6.

Temperature (°C)	Look Direction @ 2 μs Time Constant								
	1	2	3	4	5	6	7	8	9
-20	10.71	15.56	11.36	7.66	17.74	9.50	6.32	0.16	2.62
-10	13.68	18.70	14.43	11.17	20.84	12.74	9.24	2.66	6.18
0	16.89	22.23	17.44	14.54	24.13	15.85	12.24	6.48	9.70
10	21.12	25.84	21.16	19.02	27.75	19.94	15.89	10.95	13.63
20	22.48	27.47	22.53	20.32	29.01	21.36	17.16	12.70	15.39
30	24.36	29.34	24.37	22.02	30.63	23.26	18.70	14.42	17.39
	Look Direction @ 10 μs Time Constant								
	1	2	3	4	5	6	7	8	9
-20	9.75	14.79	10.66	7.07	17.12	8.80	5.52	0.08	1.78
-10	12.81	17.99	13.68	10.41	20.25	11.69	8.30	2.10	5.21
0	16.07	21.19	16.66	13.94	23.48	15.07	11.42	5.80	8.95
10	19.80	24.42	19.80	17.51	26.70	18.71	14.41	9.59	12.38
20	21.62	26.33	21.42	19.67	28.36	20.56	15.83	11.96	14.64
30	23.14	28.34	23.15	21.38	29.79	22.36	17.62	13.64	16.55
	Look Direction @ 50 μs Time Constant								
	1	2	3	4	5	6	7	8	9
-20	6.70	12.09	7.88	4.70	15.17	5.96	2.87	0.00	0.28
-10	9.61	14.91	10.87	7.97	17.98	9.20	5.26	0.51	2.64
0	12.93	18.56	13.94	11.53	21.36	12.62	8.80	3.54	6.43
10	15.89	20.95	16.54	14.97	23.80	15.22	10.98	6.44	9.32
20	18.08	23.30	18.35	17.24	25.56	17.54	12.65	9.13	11.69
30	19.44	25.16	19.97	19.66	27.24	19.01	14.16	10.80	13.31
	Look Direction @ 100 μs Time Constant								
	1	2	3	4	5	6	7	8	9
-20	5.32	10.83	6.82	3.54	13.98	4.67	1.59	0.00	0.15
-10	8.06	13.61	9.55	6.76	16.93	7.50	3.80	0.30	1.59
0	11.66	17.29	12.51	10.72	20.40	11.20	7.26	2.63	5.06
10	14.11	19.46	15.02	13.79	22.67	13.51	9.47	5.36	7.80
20	15.35	21.00	15.90	16.24	23.90	14.98	10.33	7.19	9.54
30	18.08	23.91	18.65	20.20	26.20	17.92	13.03	9.82	12.20

Table 3.1: IES #6 temperature calibrations giving the ADC channel of the pedestal position for all integration time constants (Personal Communication: Mr. Roy Cope, LANL).

3.2 IES Integration Time Constant Dependency

The integration time constant represents another critical IES feature affecting the pedestal of the IES. As table 3.1 illustrates, at a specific temperature the pedestal position decreases in histogram channel numbers as the integration time constant is increased. The FWHM of the pedestal approximately doubles when comparing the 10 μs to 100 μs integration time constants. Figure 3.2 illustrates the effects of a 10 μs histogram compared to a 100 μs histogram spectrum taken by the IES for 100 keV electrons incident at comparable rates. The pedestal position for the 10μs histogram is centered about channel

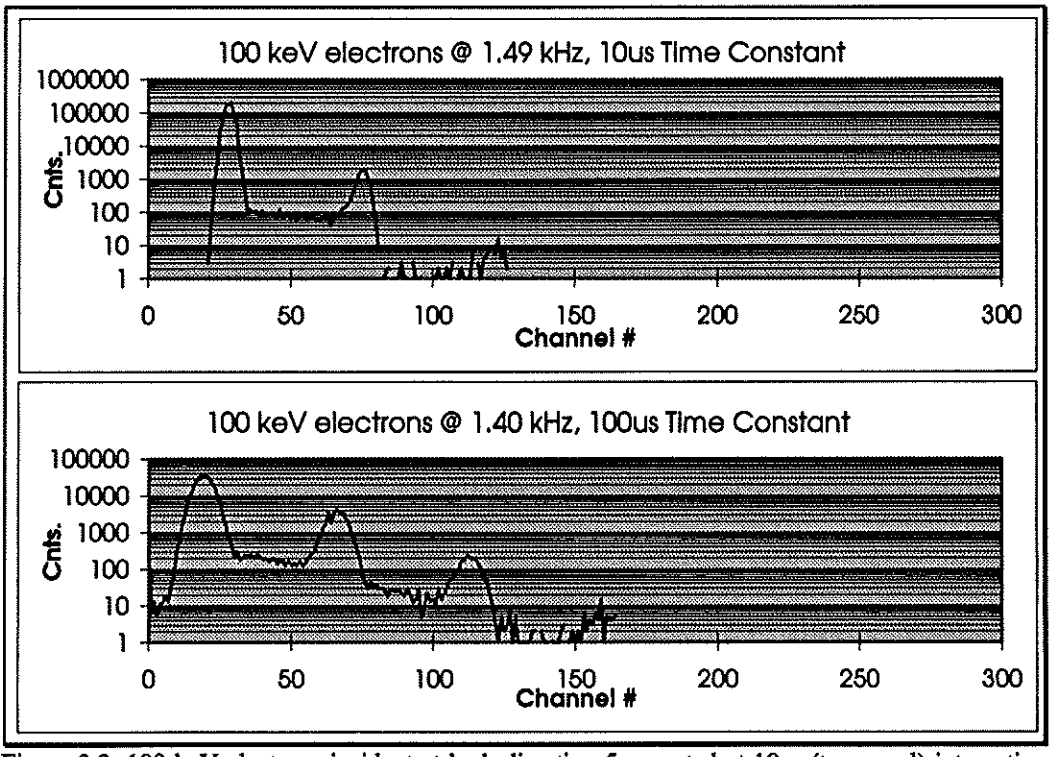

Figure 3.2: 100 keV electrons incident at look direction 5 operated at 10us (top panel) integration time, and 100us (bottom panel) integration time.

28 with a FWHM of 3.48 channels. The 100 μs histogram depicts a pedestal centered about channel 19 with a FWHM of 7.17 channels.

The shift in pedestal depicted in figure 3.2 is due to an increase in leakage currents of the MXRP input protection diodes, the coupling capacitors, and any other board leakages. As an example of this effect, the analysis of the contribution of the coupling capacitors follows as a possible major contributor. Most capacitors have an insulation resistance anywhere in the range of 10^{13} Ω to 10^{15} Ω. A 100 V voltage drop across the coupling capacitors, due to an input signal from radiation incident on the Si detectors, may produce a leakage current of 0.1 pA to 10 pA. The relation between current and charge, $i(t)=dq/dt$, results in a loss of charge due to leakage of 0.01 fC to 1 fC if integrated over a 100 μs integration time. Given that there is 1.6×10^{-19} C of charge per electron, a signal loss of 62.5 to 6250 electrons is measured from the solid state detector (Personal Communication: Dr. Steve Thomas, RAL).

With a characteristic conversion of 3.6 eV per electron hole pair (EHP) generated for Si detectors, the IES measures a degraded energy range of *3.6 eV/EHP • 62.5 EHP = 225 eV* to *3.6 eV/EHP • 6250 EHP = 22.5 keV* for a 100 μs integration time. The energy loss range for the 10 μs integration time can be similarly calculated to be 22.5 eV to 2.25 keV. Therefore, a larger loss of energy signal is expected during longer integration times resulting in a shift of the spectrum as depicted in figure 3.2. These results show that a decrease of the baseline is expected to range anywhere from 202.5 eV to 20.25 keV,

depending on the insulation resistance's of the coupling capacitors, when switching from 10 μs to 100 μs integration time. The measured shift stated earlier agrees with this result, and is shown to be approximately 9 channels, which with a measured 2.0 keV/channel gain results in a shift of 18 keV.

The MXRP becomes more sensitive to low frequency interference, such as the power supply noise and detector bias, with increase in integration time constant. This effect is revealed by the increase in FWHM with an increase in integration time constant. Figure 3.3 summarizes the effect of the time constant on instrument response from calibration data taken at Goddard Space Flight Center, and depicts a linear relationship between FWHM, Pedestal Position, and time constant of operation.

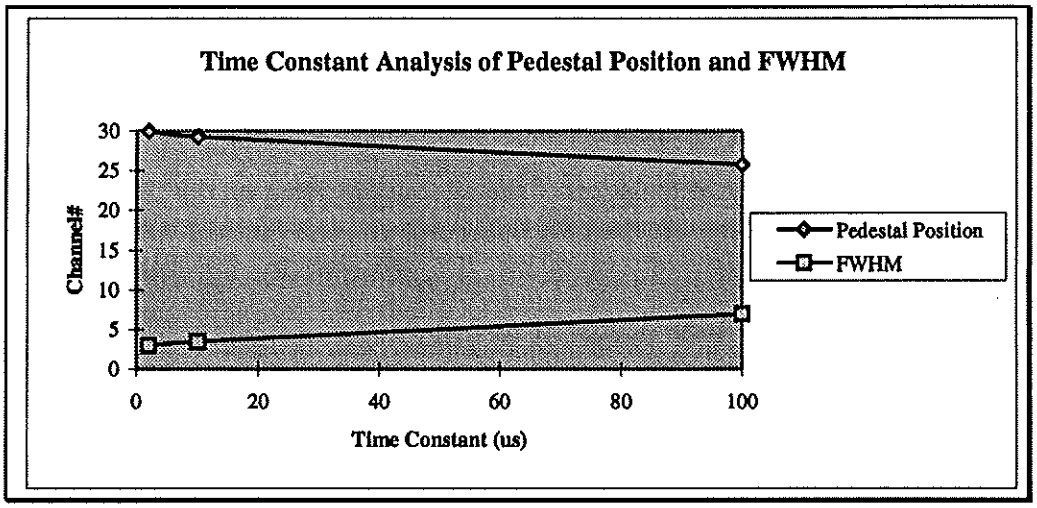

Figure 3.3: Pedestal position and FWHM dependency on the integration time constant for look direction 5 of IES# 6 measured for 2, 10, and 100 us time constants.

3.3 IES Energy and Intensity Dependency

Particle beam tests of various energies and intensities performed at Goddard Space Flight Center employing a Van de Graaf particle accelerator revealed a critical dependence

of the IES on its particle energy and intensity environment. The tests were performed by varying the intensity of a mono-energetic particle beam incident on the IES, and recording the resulting distribution in histogram mode. Table 3.2 lists the tests that were performed on IES# 6 in October of 1996.

The intensity of the incident particle beam was measured by a monitor dropped in front of the beam prior to the IES performing its data run. The monitor was a detector with a circular active area with a diameter of approximately 3.5 mm. The area of the monitor was then measured to be $\pi r^2 \approx 9.62$ mm^2. Since the aperture of the IES is approximately 2 mm^2, the intensity incident on the IES would then be equivalent to the intensity measured by the monitor divided by the conversion factor $9.62mm^2/2mm^2 \approx 4.81$. However, the beam of the Van de Graaf accelerator fluctuated approximately ±10% with time, and discrimination electronics produced an intensity reading higher than what was believed to be the true intensity. A calculation of the intensity incident on the IES was then performed by dividing the number of events the IES recorded by the total live time over the accumulation period. The occurrence of pile-up was also taken into account by realizing that one recorded event for the first pile-up was in reality two particles incident on the instrument, one recorded event for the second pile-up was in reality three particles incident on the instrument, and so on. Table 3.2 lists the calculation of the intensity for the IES performed in this manner.

The testing revealed that with increasing incident particle intensity of a mono-energetic beam, the pedestal position of the IES linearly decreases in histogram channels.

Look Direction	Time Constant (μs)	Beam Energy (keV)	Calculated Intensity (kHz)						
2	2	200	15.56	27.86					
2	10	30	0.10	0.28	2.02	4.29			
2	10	40	0.60	1.16	5.24	19.12	165.22		
2	10	100	1.11	2.16	5.49	11.10	22.68		
2	10	200	0.86	1.47	3.70	12.62			
2	100	30	0.13	0.35	0.88				
2	100	40	0.56	0.99	5.77				
2	100	100	0.14	1.04	5.11	10.33	19.21		
2	100	200	0.74	1.36	3.31				
3	2	200	5.11	12.20					
3	10	200	0.43	1.36	4.06	13.98			
5	2	200	9.13	28.02	65.42				
5	2	450	0.45	13.92	32.22				
5	10	30	0.12	0.28	1.38	2.88	9.31		
5	10	40	1.05	4.98	13.06	30.74	119.98		
5	10	60	0.52	1.35	8.12	15.30	32.58		
5	10	75	0.14						
5	10	100	0.71	1.49	7.42	18.03	23.24	47.94	
5	10	200	1.36	1.96	2.71	4.12	7.26	16.27	22.79
5	10	450	1.23	2.78	10.84				
5	100	30	0.15	0.44	1.19	1.86			
5	100	40	0.27	1.01	4.16				
5	100	60	0.46	1.26	7.78	15.06	19.04		
5	100	100	1.40	7.17	12.08				
5	100	200	0.10	0.34	0.66	1.34	2.63	6.38	
5	100	450	0.19	0.82					
8	2	30	0.10	0.20	1.92				
8	2	198	5.41						
8	10	30	0.11	0.27	1.32	2.64	8.38	24.05	
8	10	40	0.36	0.68	3.41	12.63	117.77		
8	10	60	0.38	1.11	1.95	5.11	12.14	46.46	
8	10	198	0.83	1.80	4.27				
8	100	30	0.12	0.38	2.51				
8	100	40	0.32	0.67	2.83				
8	100	60	0.37	1.85	4.49	11.39			
8	100	198	0.35	0.67					

Table 3.2: Summary of Goddard Space Flight testing during October 1996 of IES# 6.

Figure 3.4 illustrates the intensity and energy dependency of the IES from the data given in table 3.2 for look direction 5 operating with a 10 μs integration time constant. The top panel reveals a linear dependency of the IES pedestal position to incident particle intensities for various mono-energetic particle beam tests. Linear characterization of the intensity dependencies for all energy tests reveals a linear dependency for the pedestal position as a function of particle energy (bottom panel). These dependencies are explained through the AC coupling data accumulation the IES performs.

Events which occur during the IES integration time period are associated with an amplitude which is proportional to the deposited energy of the incident radiation. Since this is an AC coupled signal there is a negative exponential return to the baseline associated with it, as illustrated in figure 3.5. The exponential decay time of the return signal is typically much longer than the integration time period, and makes a small contribution to the signal integrated over the time constant compared to the amplitude of the event (Personal Communication: Dr. Steve Thomas, RAL).

Figure 3.5 illustrates the response of the IES to incident radiation. T_{i1} and T_{r1} represent the integration period and the 48 μs dead time for the first cycle, respectively. A signal is coupled over the integration time period T_{i1}. Its measurement is the integration over the entire signal which also has a negative contribution during its return decay time. This negative effect is small if a small integration time is chosen compared to the time constant associated with the exponential decay. The exponential decay time constant should ideally be large enough to distribute its effect over as long a time scale as possible in

order to minimize its impact on the sample period. However, as the rate is increased the second dead time cycle, T_{r2}, illustrates how the amplitude measurement may appear to shift in energy when two return signals contribute to drive down the apparent baseline (Perry, 1996).

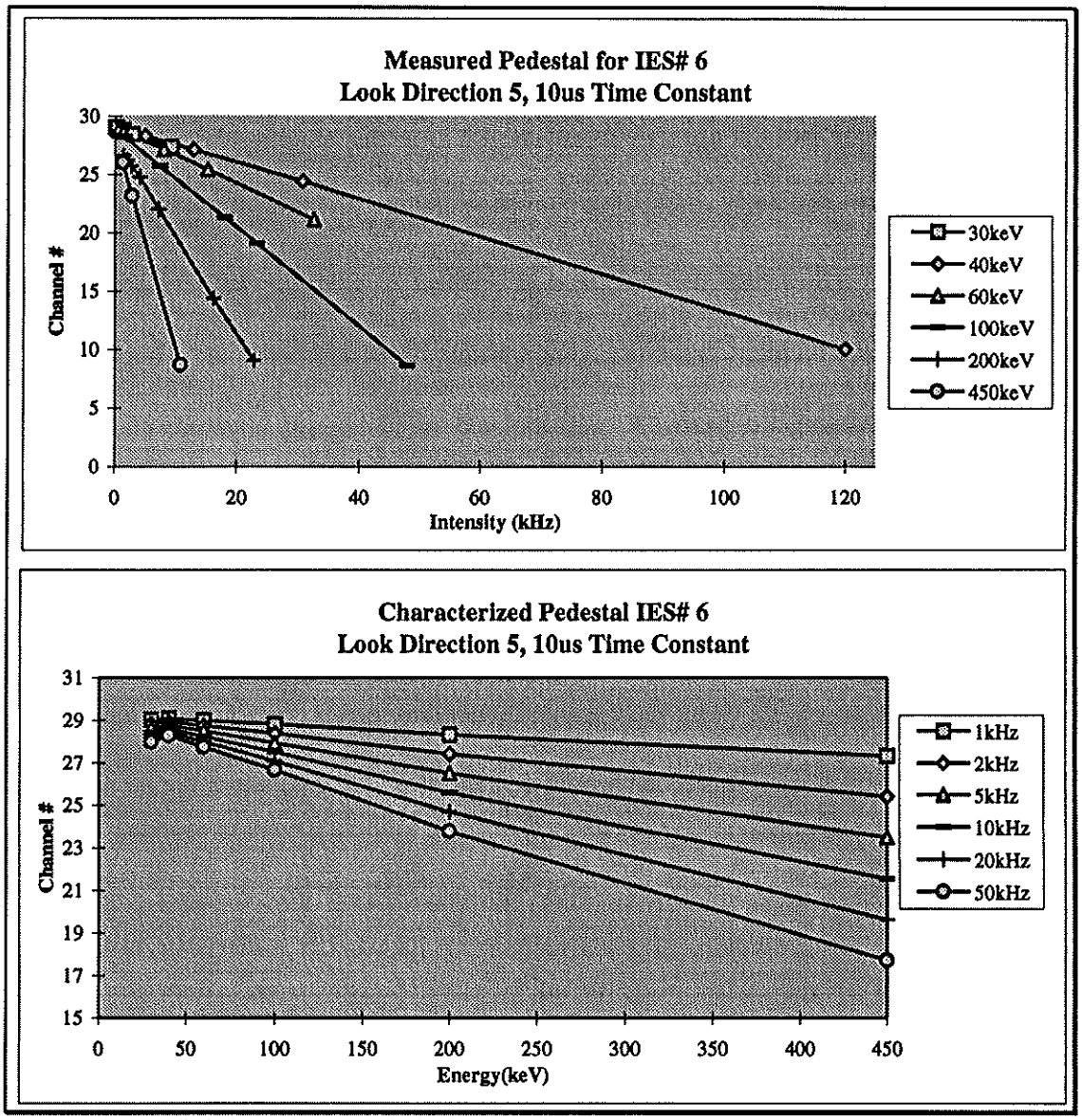

Figure 3.4: IES# 6 dependency analysis for intensity (top panel) and energy (bottom panel) for look direction 5 operated at 10us integration time constant.

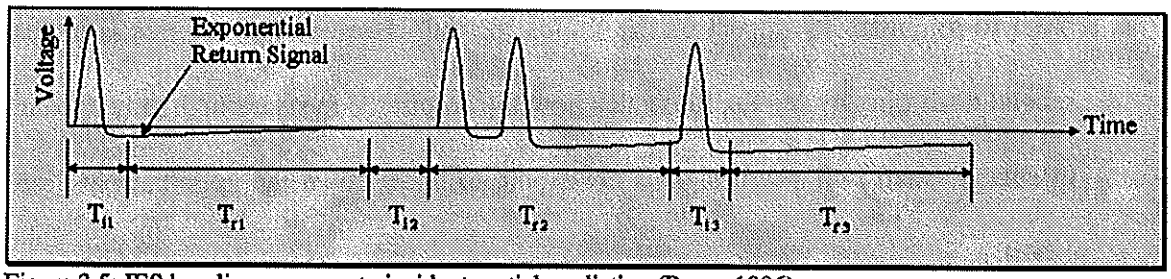

Figure 3.5: IES baseline response to incident particle radiation (Perry, 1996).

3.4 IES Gain Analysis

Throughout the dependencies referred to in this chapter, the IES gain has remained relatively constant. This indicates the effects of the operating mode and environment on instrument performance as uniform with respect to energy. Table 3.3 shows calculated gains from the incident mono-energetic particle beam and pedestal. This is done such that for a mono-energetic beam, E, accumulated in histogram channel, C_E, and a pedestal accumulated in histogram channel, C_P, the Gain can be calculated as $G_{IES} = E/(C_E - C_P)$. Low energy gains appear to be higher as a result of low end pedestal effects upon mono-energetic beam peak determination. The high end pedestal counts are assimilated with the low end beam counts to produce a mono-energetic beam centroid positioned lower in the histogram spectrum. This effect would decrease $C_E - C_P$ to render a higher apparent gain.

2 μs Integration Time Constant			
200 keV		450 kev	
Intensity (kHz)	Gain (keV/Ch)	Intensity (kHz)	Gain (keV/Ch)
9.13	2.09	4.69	2.10
28.02	2.08	13.92	2.11
65.42	2.08	32.22	2.11

10 μs Integration Time Constant					
30 keV		40 keV		60 keV	
Intensity (kHz)	Gain (keV/Ch)	Intensity (kHz)	Gain (keV/Ch)	Intensity (kHz)	Gain (keV/Ch)
0.12	4.66	1.05	2.66	0.52	2.29
0.28	3.59	4.98	2.68	1.35	2.28
1.38	3.62	13.06	2.68	8.12	2.30
2.88	3.63	30.74	2.71	15.30	2.30
9.31	3.62	119.98	2.74	32.58	2.29
100 keV		200 keV		450 keV	
Intensity (kHz)	Gain (keV/Ch)	Intensity (kHz)	Gain (keV/Ch)	Intensity (kHz)	Gain (keV/Ch)
0.71	2.11	1.36	2.08	1.23	2.10
1.49	2.12	1.96	2.08	2.78	2.10
7.42	2.12	2.71	2.09	10.84	2.11
18.03	2.13	4.12	2.09		
23.24	2.12	7.26	2.08		
47.94	2.13	16.27	2.08		
		22.79	2.07		

100 μs Integration Time Constant					
30 keV		40 keV		60 keV	
Intensity (kHz)	Gain (keV/Ch)	Intensity (kHz)	Gain (keV/Ch)	Intensity (kHz)	Gain (keV/Ch)
0.15	3.13	0.27	2.74	0.46	2.33
0.44	3.18	1.01	2.76	1.26	2.33
1.19	3.12	4.86	2.82	7.78	2.29
		13.47	2.59	15.06	2.36
				19.04	2.35
100 keV		200 keV		450 keV	
Intensity (kHz)	Gain (keV/Ch)	Intensity (kHz)	Gain (keV/Ch)	Intensity (kHz)	Gain (keV/Ch)
1.40	2.14	0.10	2.10	0.19	2.10
7.17	2.15	0.34	2.10	0.82	2.11
12.08	2.13	0.66	2.10		
19.18	2.15	1.35	2.10		
		2.63	2.11		
		6.38	2.12		

Table 3.3: IES# 6, look direction 5 gain analysis.

Chapter Four

IES Historical Missions Review

4.1 Pulsaur II Mission

The IES was launched on a rocket mission designated Pulsating Aurora II (PULSAUR II) on February 9, 1994 from the Andoya Rocket Range in Norway. The PULSAUR II was a joint venture between NASA and the Norwegian Space Agency, and was commissioned to obtain information about pulsating auroras. The mission comprised a payload for measurements of electrons and ions as a function of energy and pitch angle, optical emissions, X-rays, DC electric and AC electromagnetic fields, and electron densities and temperatures (Young, 1996). Two IES units were launched, one utilizing a Hughins chip in place of the MXRP, and one utilizing the MXRP chip operated only in the 100 μs time constant (Levine, 1994). A thesis authored by Levine (1994) analyzed the performance of both instrument versions. The Hughins version had no data return as a result of inappropriate electrical configuration aboard the rocket. However, the MXRP version returned data which indicated for the first time that the functionality of the IES described in chapter 3 was not clearly understood.

4.2 Polar Mission

The Polar spacecraft was developed under the NASA Global Geospace Science (GGS) mission. Polar was launched on February 24, 1996 on a Delta II launch vehicle out of Vandenberg Air Force Base. Polar is currently generating data which examines in part

the polar regions of the Earth's magnetosphere with a variety of instruments, including the IES, capable of studying energetic particles, magnetic and electric fields, and imaging auroral regions (Young, 1996). Figure 4.1 depicts the spacecraft with its compliment of instruments.

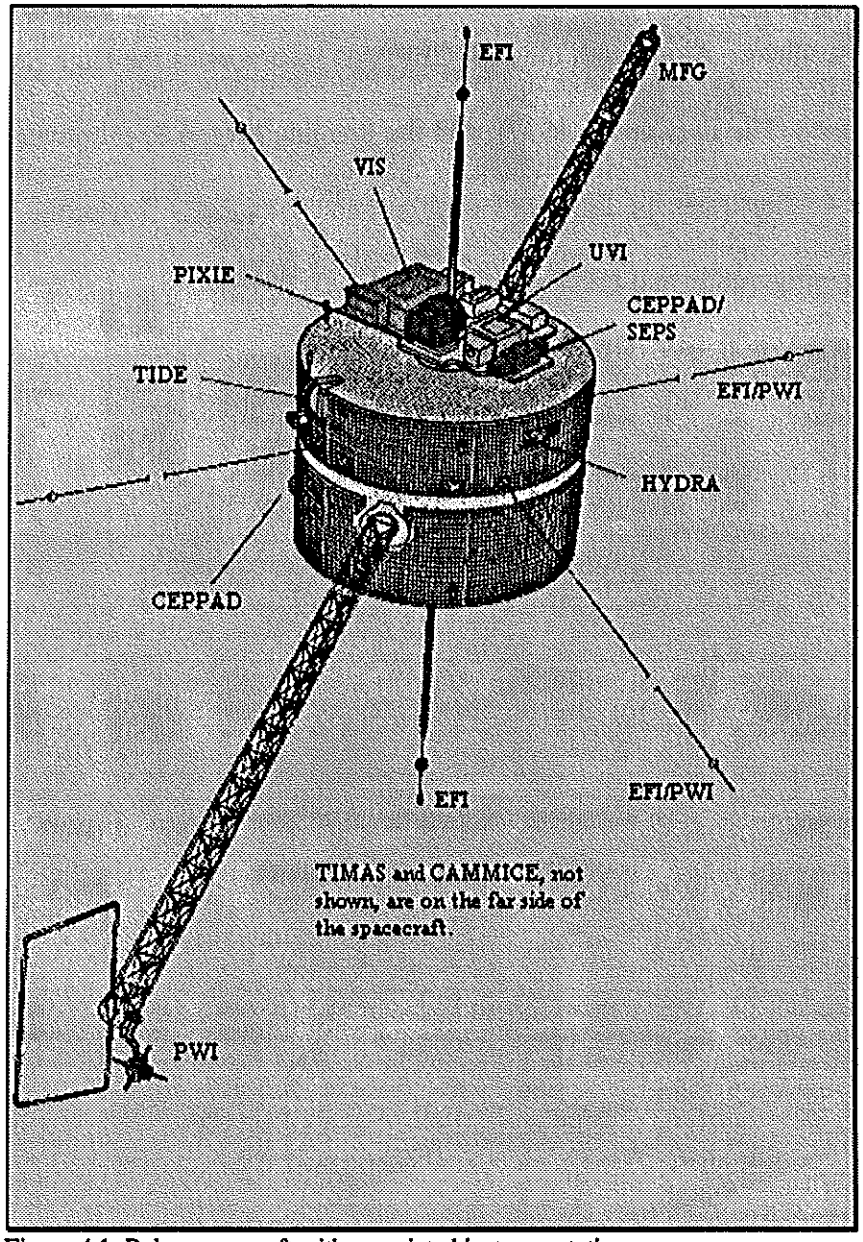

Figure 4.1: Polar spacecraft with associated instrumentation.

The IES on Polar is part of the Comprehensive Energetic Particle and Pitch Angle Distribution (CEPPAD) experiment (Blake, et al., 1995). All aspects of the IES instrument response and configuration aboard Polar are identical as to what has been mentioned thus far. However, the addition of a small element Si detector of 0.68 mm^2 has been placed along side each side element for the measurement of high particle fluxes in the magnetosphere. Along with the IES, CEPPAD incorporates the High Sensitivity Telescope instrument (HIST) (Contos, 1997), and the Imaging Proton Spectrometer instrument (IPS). Figure 4.2 illustrates the IES/HIST configuration for CEPPAD with the IES situated on top of the configuration and HIST positioned below.

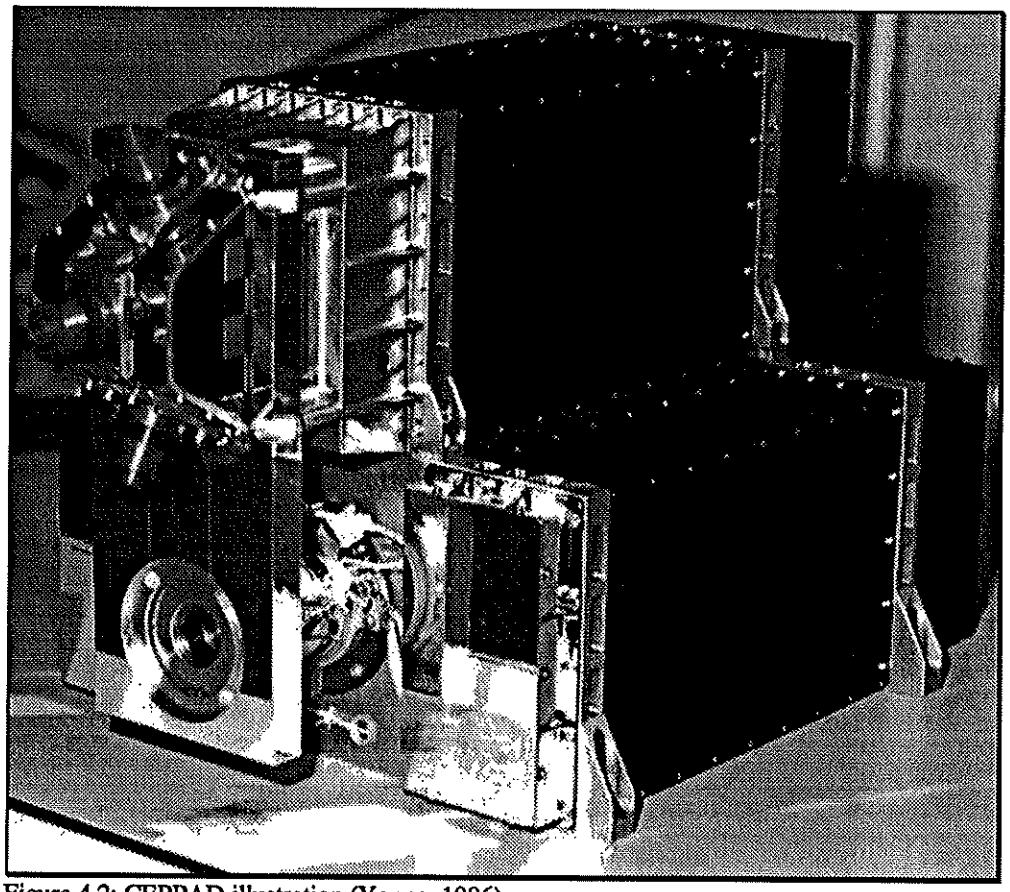

Figure 4.2: CEPPAD illustration (Young, 1996).

A representation of two of Polar's orbits is given in figure 4.3a. Shown is its orbital path in the solar magnetic coordinate system from January 9, 1997, 15:12 universal time (top panel), to January 11, 1997, 02:12 universal time (bottom panel). This provides Polar's position for the entire period of January 10,1997 when a coronal mass ejection (CME) from the sun was encountered by Polar's compliment of instruments. To better understand the data returned by the IES, it is necessary to understand its orientation on Polar with respect to its environment. Figure 4.3b displays the orientation of the IES aboard Polar with the represented polar spin axis directed perpendicular to its orbital plane shown in figure 4.3a. As a result of this orientation, look directions 1 and 9 have the smallest roll modulation due to the spacecraft spin, and remain mostly aligned 90° with respect to the earth's magnetic field, $\vec{B}$. Conversely look direction 5 has the largest roll modulation, and as a result samples the largest range of pitch angles, angles between the particle velocity vector, $\vec{v}$, and the local magnetic field vector, $\vec{B}$.

As mentioned earlier, the IES sorts the measurements accumulated over a spin into 16 sectors for each look direction. Therefore, each sector represents a spacecraft spin of 360°/16 = 22.5°. Taking into consideration the 9 look directions, which measure 180°, the spatial sphere the IES measures divides into 144 elements, each 22.5° x 20°. Figure 4.4 illustrates the IES sectored data for look directions 1 through 5 for 250 keV electrons. The lines crossing through the high intensity measurements recorded at approximately 07:00 UT represent the alignment of the 90° vector to the magnetic field vector. This alternating

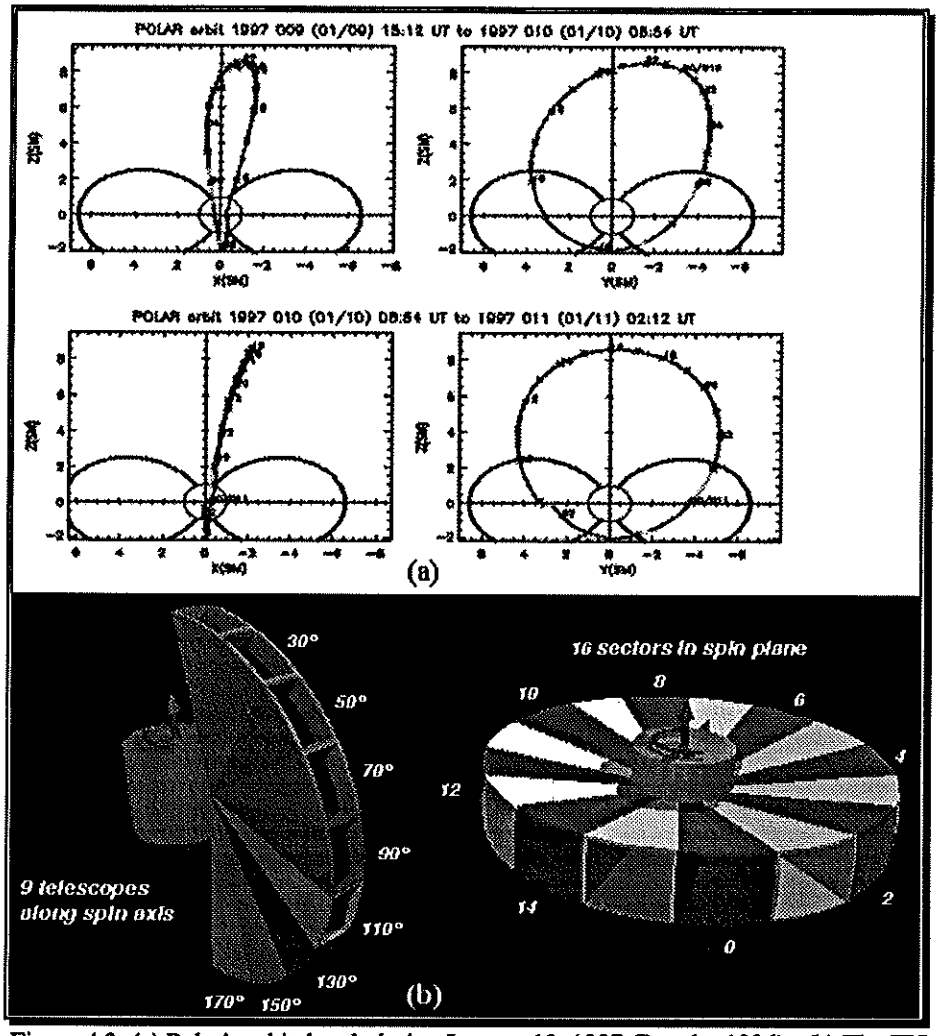

Figure 4.3: (a) Polar's orbital path during January 10, 1997 (Peredo, 1996). (b) The IES orientation and sectorization layout for all look directions relative to Polar's spin axis (Henderson, 1996).

sector intensity for look direction 5 (top panel) represents the loss cone, cone represented by the particle pitch angle for which low particle intensity is present, as it senses for particles along the magnetic field line (minimum intensity), and perpendicular to the magnetic field line (maximum intensity). Look direction 1 (bottom panel) only senses for particles perpendicular to the field line, thus never displaying a diminished particle intensity as is seen for magnetic field aligned sectors.

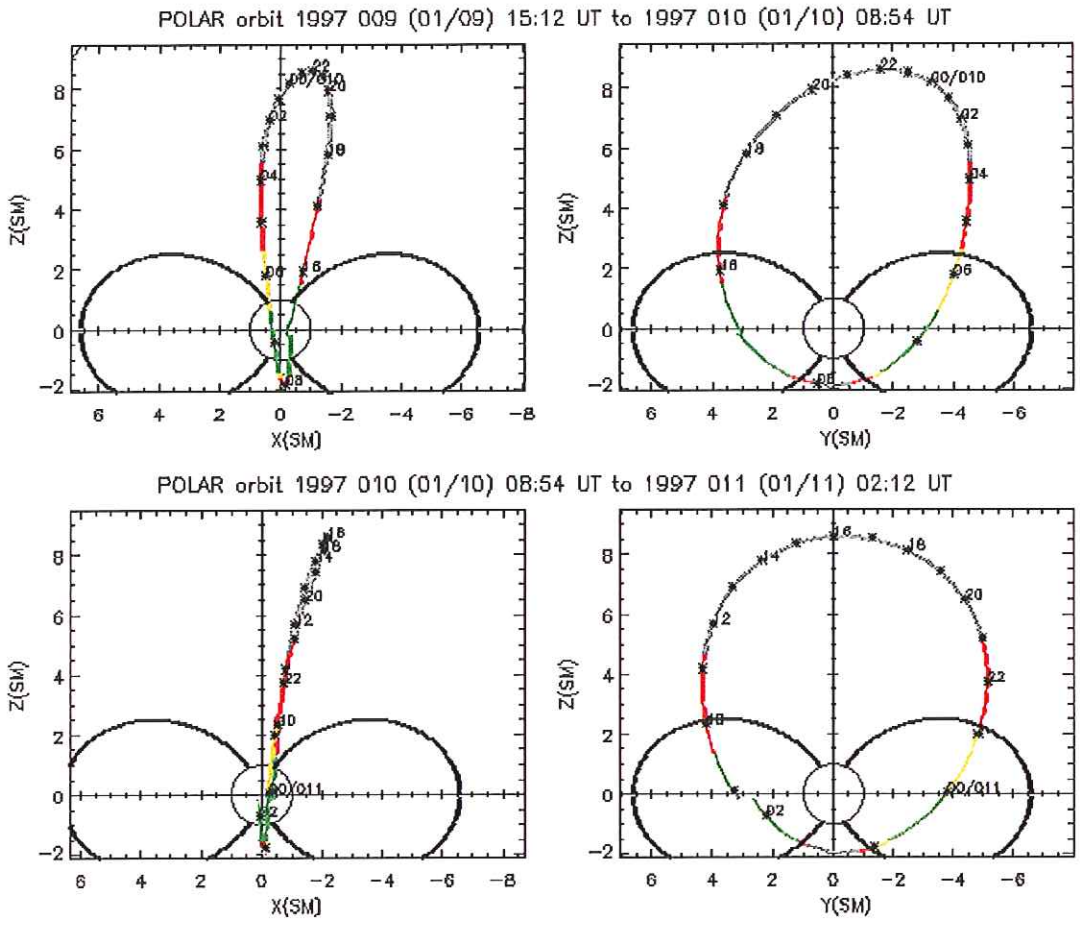
POLAR orbit 1997 009 (01/09) 15:12 UT to 1997 010 (01/10) 08:54 UT
Z(SM)
X(SM)
Y(SM)
POLAR orbit 1997 010 (01/10) 08:54 UT to 1997 011 (01/11) 02:12 UT
Z(SM)
X(SM)
Y(SM)

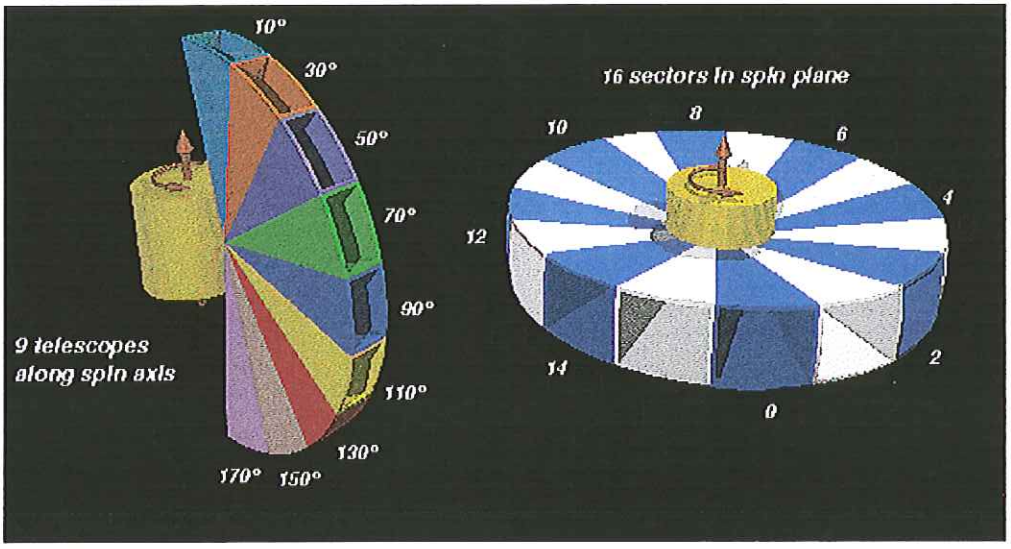
10°
30°
50°
70°
90°
110°
130°
150°
170°
9 telescopes
along spin axis
16 sectors in spin plane

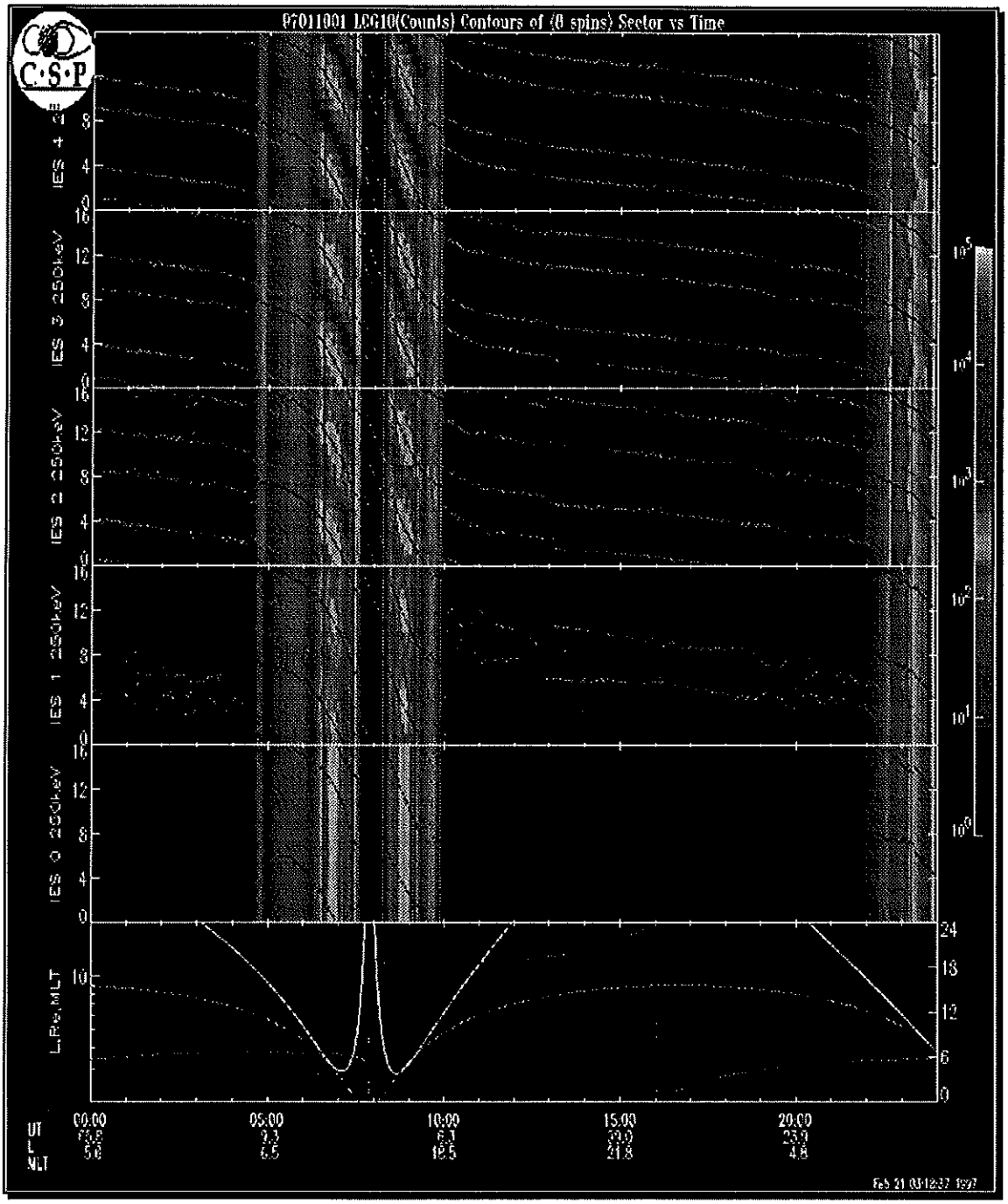

Figure 4.4: IES sectored data for January 10, 1997. IES 0 to IES 4 represent look direction 1 to 5 respectively.

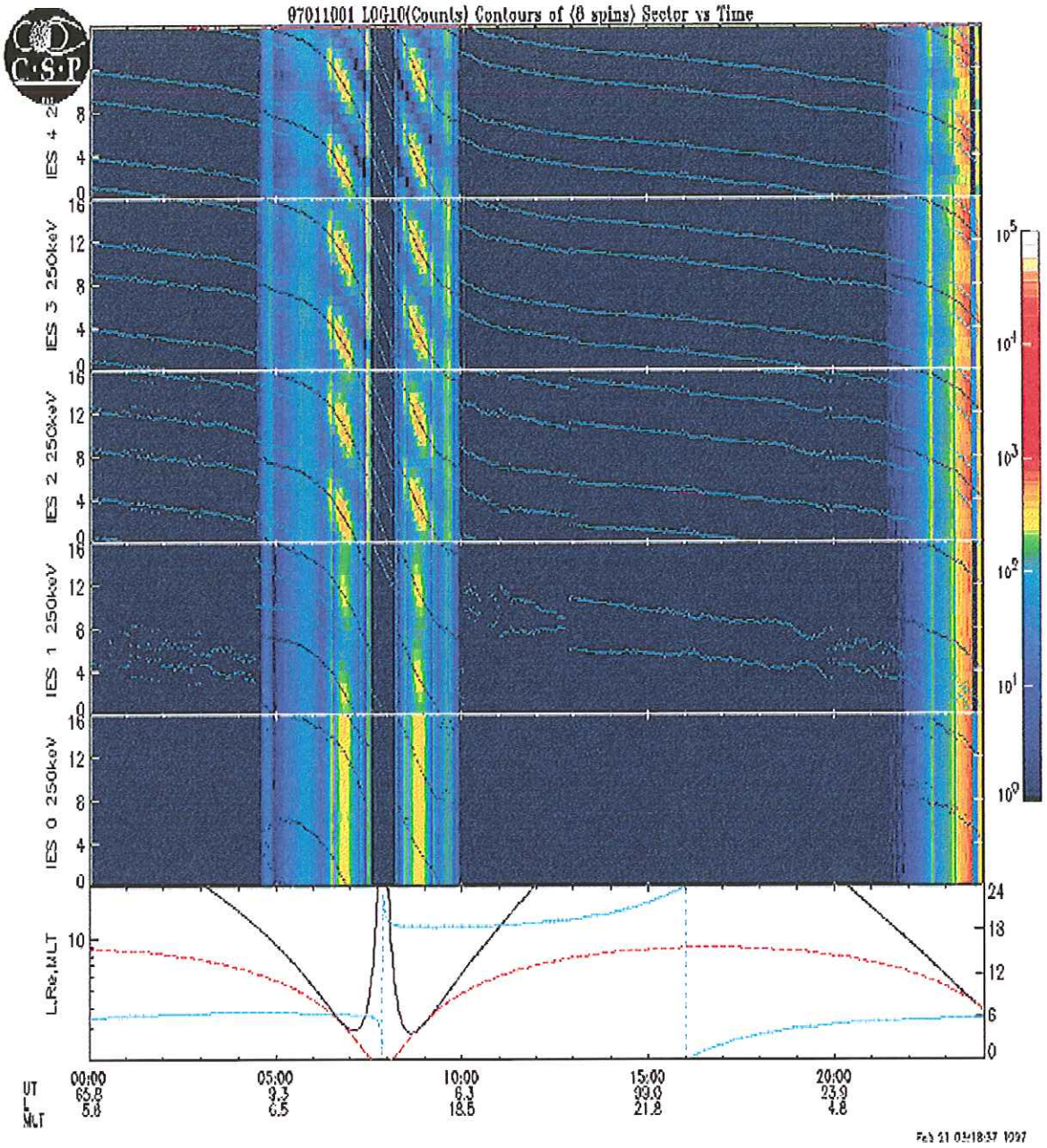
97011001 LOG10(Counts) Contours of (8 spins) Sector vs Time
C·S·P
IES 4 250keV
IES 3 250keV
IES 2 250keV
IES 1 250keV
IES 0 250keV
L,Re,MLT
UT
MLT
00:00
05:00
10:00
15:00
20:00
65.8
9.3
6.3
99.0
23.9
5.8
6.5
18.5
21.8
4.8

Figure 4.5 illustrates, for look direction 5, the procedure followed for reducing the IES data returned from orbit into meaningful scientific data without corruption due to instrument dependencies on operational modes and particle environments. The top panel represents spin averaged counts per energy channel for 16 spins. The most intense horizontal line centered about energy channel 3 represents the pedestal. The pedestal is observed to shift from the third energy channel to the second during high intensity radiation apparent just after 06:00 UT and just prior to 09:00 UT. These energy channels are a linear representation of the 16-bin mode data. The second panel from the top utilizes the geometric factor of the instrument to normalize for detector and aperture area of the instrument, and re-plots the top panel. Panel three normalizes panel two for instrument passband energies, and panel four reduces panel three to per unit time in seconds, which for Polar is represented by 6 seconds per spin. Panel five sums the data for 16 spins for sector 5 only, sectors labeled 1 to 16, and subtracted the pedestal. The data is then normalized by the geometric factor, adjusted for instrument passband, and averaged per unit time of data acquisition. Panel six illustrates the re-sampled data from panel five to adjust for the instrument baseline offset, i.e. pedestal shift.

Figure 4.6 depicts the comprehensive CEPPAD analysis of the center elements after data normalization for instrument dependencies. The first three panels from the top, look directions 2, 5, and 8 respectively, illustrate the electron intensity distribution for energies ranging from 30 to 400 keV during the January 10th CME event. The fourth panel

illustrates the sectored data for look direction 5, and the bottom panel illustrates data from the IPS.

Figure 4.3a illustrates Polar entering the radiation belts shortly prior to 06:00 UT, proceeding out of the radiation belts and into the southern pole region shortly following 07:30 UT. Polar then reentered the day-side radiation belts at approximately 08:30 UT, and exited at approximately 10:00 UT. These time frames correspond with the measured increased intensity of energetic particles integrated over all look directions as is illustrated in figure 4.6. This synopsis demonstrates the IES performance with regard to the predicted response within earth's magnetospheric environment.

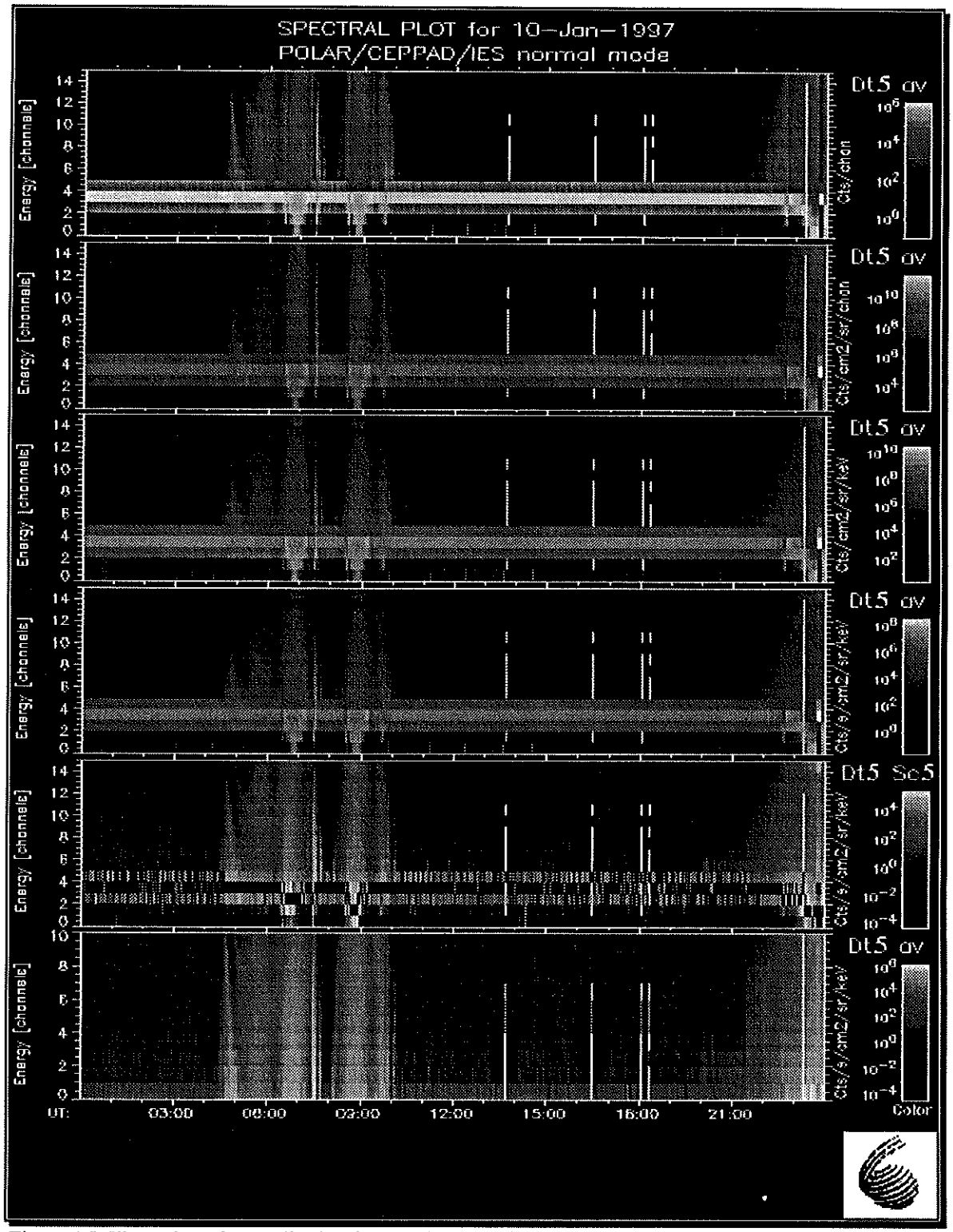

Figure 4.5: Illustration of normalization for IES dependencies on operational modes and particle environments (Carter, 1997).

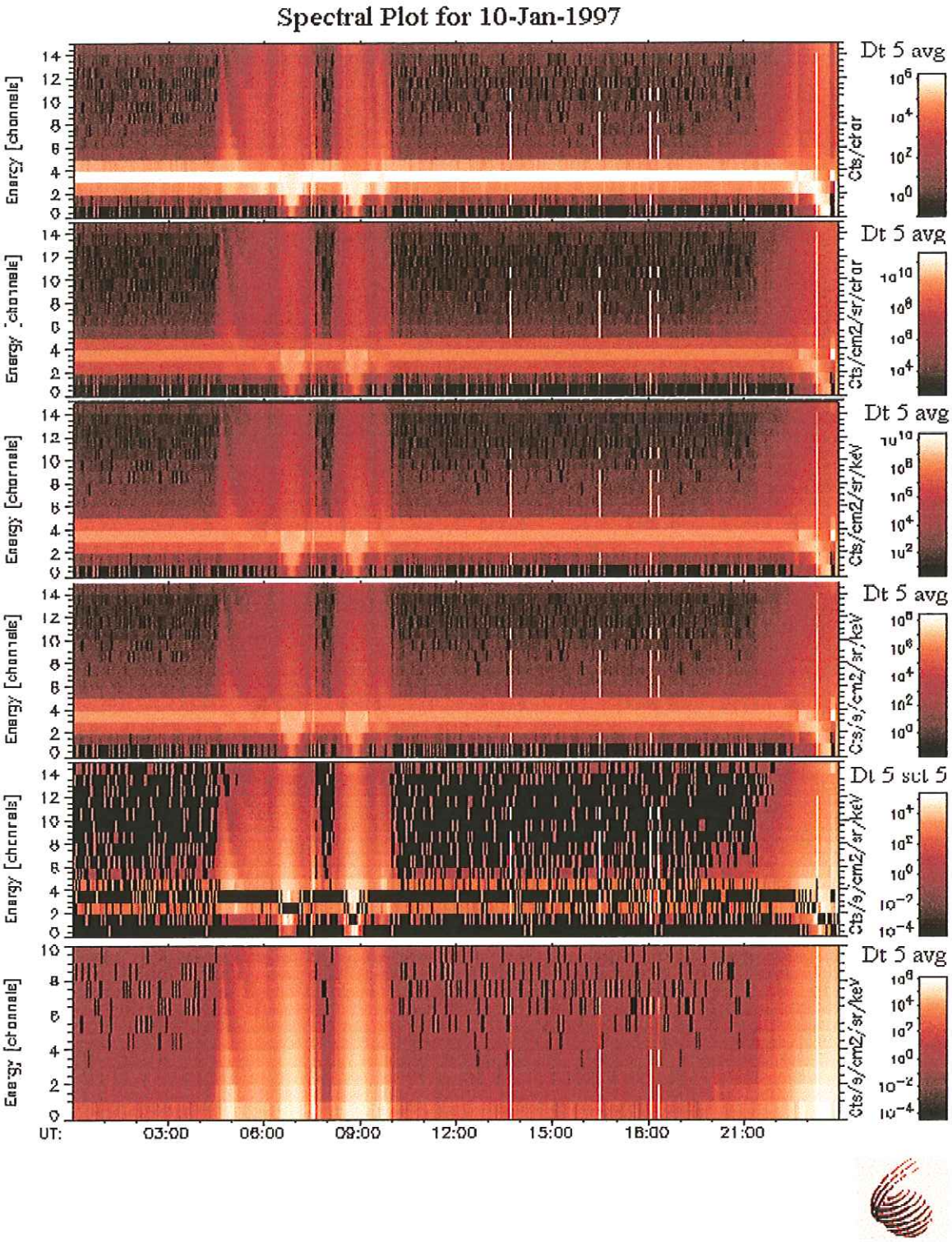
Spectral Plot for 10-Jan-1997
Energy [channels]
Dt 5 avg
Cts/cfar
Dt 5 avg
Cts/cm2/sr/cfar
Dt 5 avg
Cts/cm2/sr/kev
Dt 5 avg
Cts/s/cm2/sr/kev
Dt 5 sct 5
Cts/s/cm2/sr/kev
Dt 5 avg
Cts/s/cm2/sr/kev
UT:
03:00
06:00
09:00
12:00
15:00
18:00
21:00

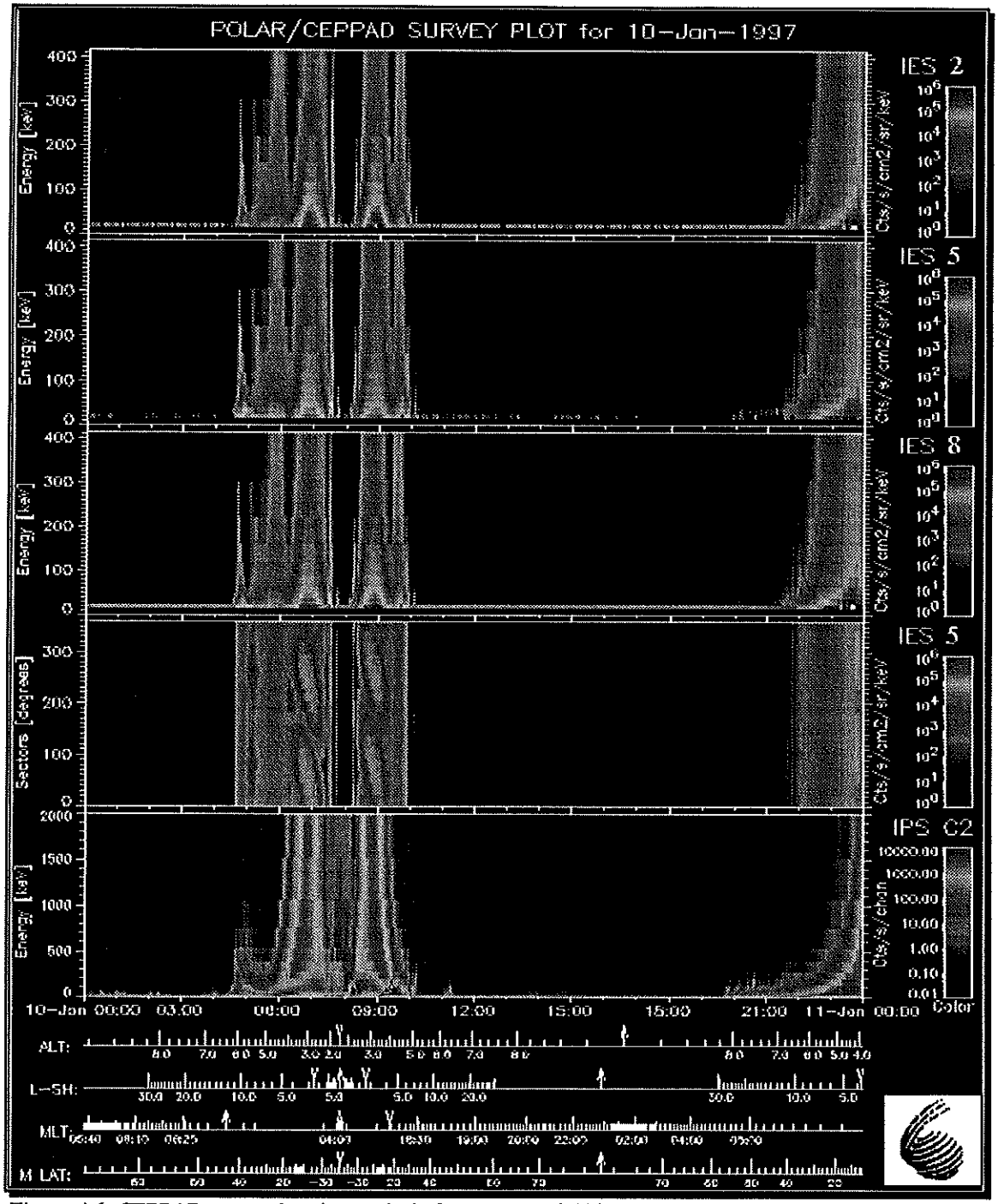

Figure 4.6: CEPPAD comprehensive analysis for January 10,1997. From top: IES energy spectrogram for look direction 2, 5, and 8 respectively, IES sectored data for look direction 5, and IPS energy spectrogram (Carter, 1997).

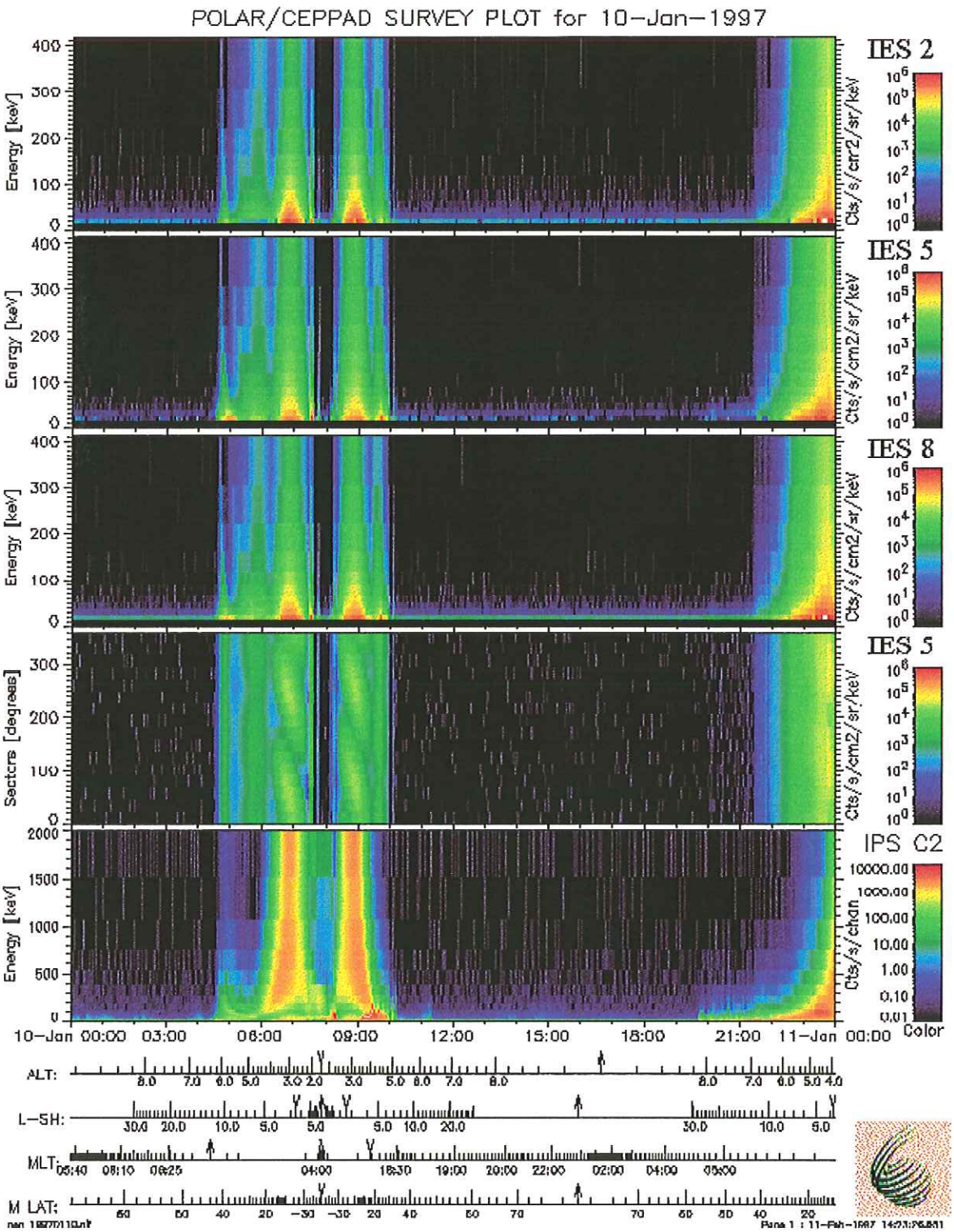
POLAR/CEPPAD SURVEY PLOT for 10-Jan-1997
IES 2
IES 5
IES 8
IES 5
IPS C2
Energy [keV]
Sectors [degrees]
Cts/s/cm2/sr/keV
Cts/s/chan
Color
10-Jan 00:00 03:00 06:00 09:00 12:00 15:00 18:00 21:00 11-Jan 00:00
ALT:
L-SH:
MLT:
M LAT:

4.3 Cluster Mission

The Cluster spacecraft was developed under the international venture known as International Solar Terrestrial Physics (ISTP) program. Cluster represented four identical spacecraft developed to examine the interaction between the Earth's magnetic field and particles from the Sun. This multi-spacecraft configuration allowed a correlation of measurements presented by the Cluster instrumentation over a spatial coordinate allowing to separate from spatial and temporal effects. Cluster was launched on June 4, 1996 on an Ariane-5 launch vehicle out of Kourou, French Guiana. The rocket was detonated approximately 40 seconds after launch because of a malfunction in the attitude control system (Young, 1996). Figure 4.7 depicts two of the four Cluster spacecraft mounted on top of one another.

The IES on Cluster is part of the Research with Adaptive Particle Imaging Detectors (RAPID) experiment (Wilken, et al., 1997). Along with the IES, RAPID incorporates the Imaging Ion Mass Spectrometer (IIMS), which measures ion-distribution functions from 30-1500 KeV/q with mass discrimination. Figure 4.8a illustrates one of the Cluster satellites with it's payload, along with RAPID, and figure 4.8b depicts the RAPID instrument (IES positioned along the right side, and the IIMS positioned on the left side of RAPID).

The functionality of the IES aboard RAPID is not dissimilar from that on CEPPAD. Its methodology of energetic particle analysis remains its objective on Cluster as it has on Polar. However, during the Integrated Systems Tests (IST's) performed in Kourou, French Guiana an excessive noise was detected for the 50 μs and 100 μs time constants.

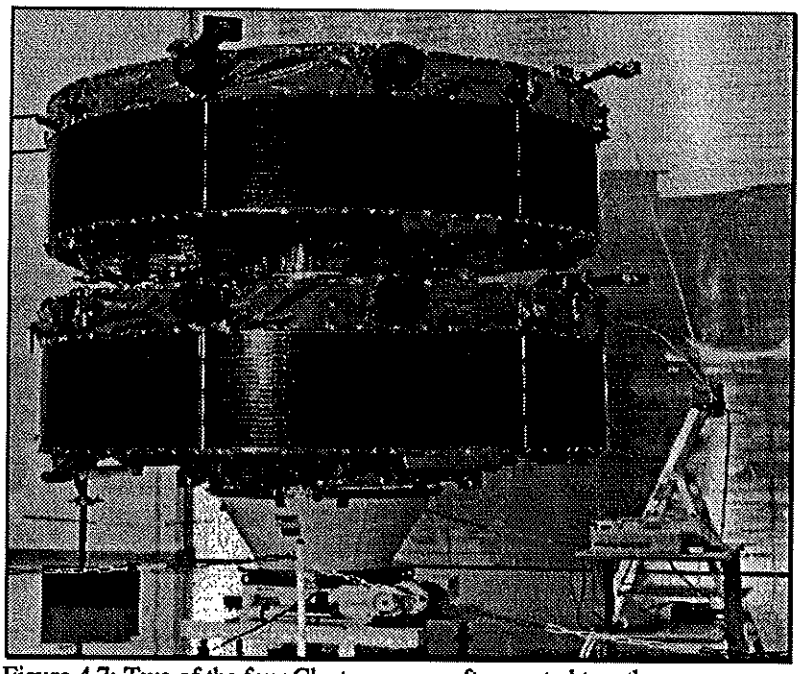

Figure 4.7: Two of the four Cluster spacecraft mounted together.

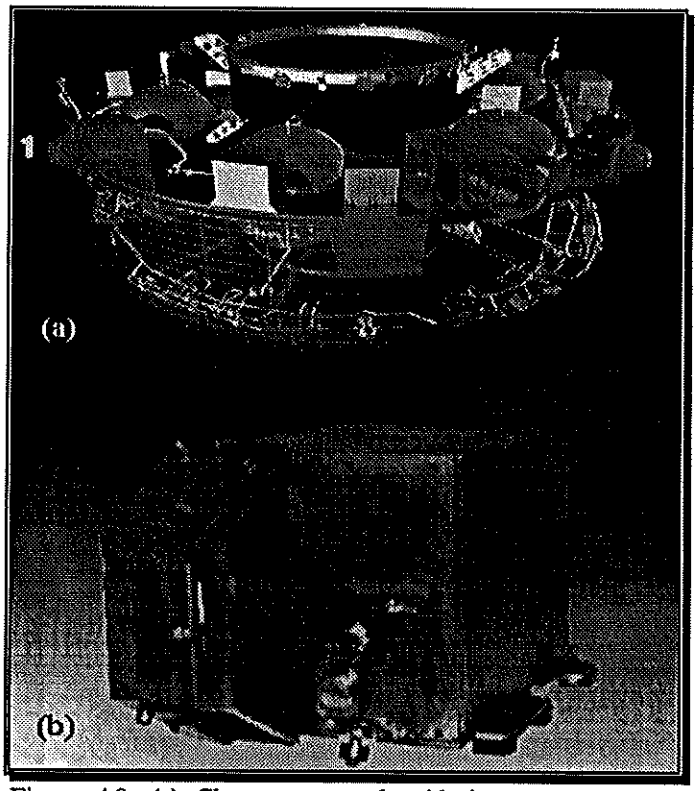

Figure 4.8: (a) Cluster spacecraft with instruments, RAPID appears as '1'. (b) RAPID instrument

A Eu-155 radioactive source was used to emit 43.47 keV, 86.60, keV, 105.36keV X-rays. Figure 4.9 illustrates the IST for look direction 5 for all integration time constants. The instrument noise progression for look direction 5 is apparent when all three source energies are distinguishable for 2 μs and 10 μs time constants, while the 50 μs and 100 μs time constants are too noisy to distinguish any source line. The cause of the excessive noise was later determined to be a result of poor filtration of the 5 V supply to the MXRP.

During periods of data readout a small current is induced based on the data output from the ADC. Assuming an output of 00001111 from the ADC, a 2 mA current is induced in the data lines. With the power supply and cable resistance adding to be roughly 0.1 Ω, a $2\ mA \bullet 0.1\ \Omega = 200\ \mu V$ voltage drop from the 5 V power supply is seen by the IES/MXRP. Assuming a rough total decoupling capacitance of 25 μF on the IES board, a rise of 200μV with a time constant of $0.1\ \Omega \bullet 25\ \mu F = 2.5\ \mu s$ occurs for the 5 V supply after data lines go to 00000000. The MXRP is then designed to start the integration of charge 4 μs after data read-out is completed. At the completion of the 4 μs the power supply will have risen by $200\mu V(1 - e^{-\frac{4\mu}{2.5\mu}}) \approx 160\mu V$. The power supply will rise the remaining 40 μV during the integration of charge. Assuming the detector and board parasitic capacitance sum to approximately 25 pF, a charge of $40\ \mu V \bullet 25\ pF = 1\ fC$ will be injected into the MXRP inputs via C_f shown in figure 1.4. This is equivalent to injecting $1\ fC/1.6\times10^{-19}\ C \approx 6250$ electrons into the MXRP inputs, or detecting a $3.6\ eV/EHP \bullet 6250\ electrons = 22.5\ keV$ particle (Personal Communication: Dr. Steve Thomas, RAL).

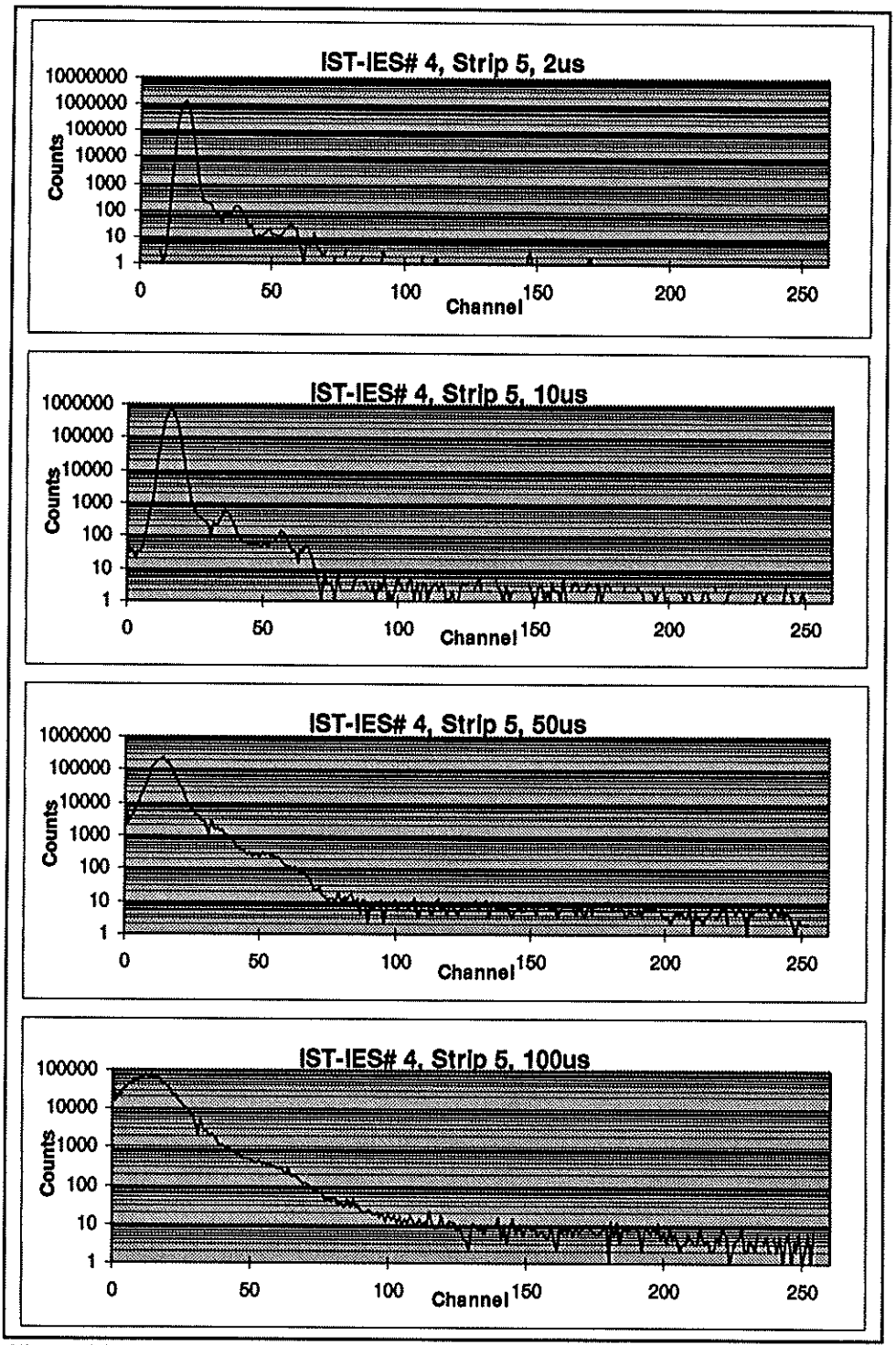

Figure 4.9: Integrated System Test (IST) in Kourou, French Guiana of IES# 4 for all integration times.

The energy of the apparent detected particle varies with the data outputs during ADC read-out. Therefore, the data itself will determine noise variation. Due to the more random nature of the signal during longer time constants, the effect of the high frequency noise worsens as the time constant of operation increases. An RC filter has been added to the electronics of IES# 6 in order to negate the effect of high frequency noise coupling into the IES coupling capacitor. Testing of IES #6 after the addition provided results of decreased noise for all integration time constants. Section 4.4 provides the analysis of the improved noise performance of the IES after the modification.

4.4 Phoenix Mission

The Phoenix mission was instituted after the Cluster failure on June 4, 1996. Phoenix will comprise one cluster satellite with its full compliment of instrumentation. Phoenix is currently scheduled to be launched on an Ariane-4 launch vehicle sometime in December of 1997. IES# 6 has been implemented as the Phoenix, RAPID contribution. All calibration prepared in this document has been done utilizing calibration testing of IES# 6 at Goddard Space Flight Center.

Radioactive source tests were performed on the IES after redelivery from Inst. f. Datenverarb. Anlagen (IDA) in Brauschweig, Germany with DPU modifications for bin definition look up tables discussed in chapter two, and the addition of a high frequency noise filter mentioned in the previous section. Two Gd-153 sources were implemented utilizing the 42 keV, 100 keV, and 141 keV lines as a calibrated source. Figure 4.10

displays the results for look direction 5 at all time constants for comparison with figure 4.9, and reflects the improved instrument noise performance. With respect to the IST's performed in Kourou, noise performance improved from pedestal FWHM of 6.57 keV to 6.35 keV, 8.52 keV to 7.71 keV, 16.70 keV to 13.17 keV, and 34.94 keV to 19.42 keV for the 2 μs, 10 μs, 50 μs, and 100 μs time constants respectively.

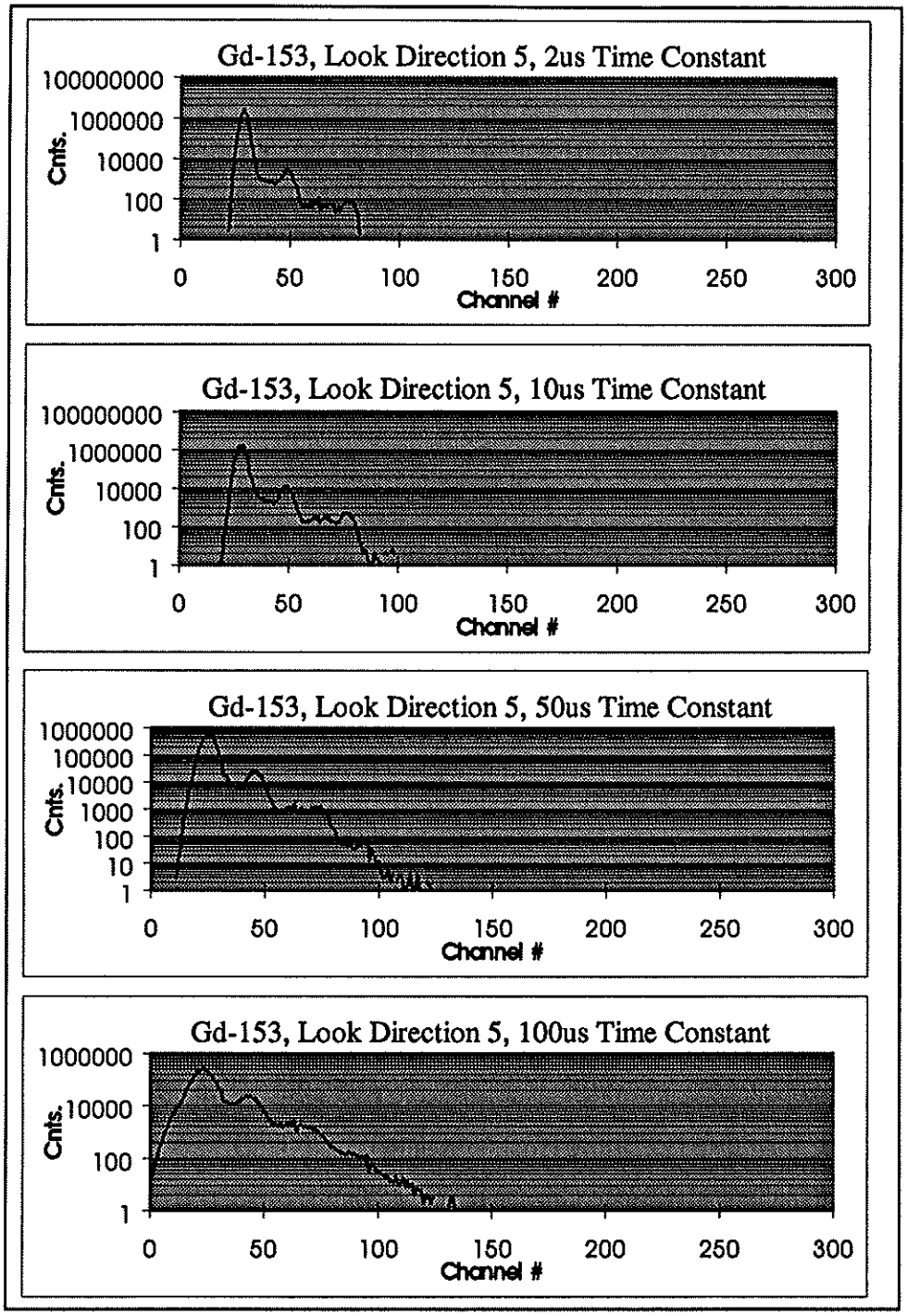

Figure 4.10: Gd-153 tests at MPAE for IES# 4 for all integration times.

Chapter Five

IES Parameterization

5.1 Pedestal Centroid Position Characterization

Chapter three discussed the dependencies of the IES on the operating temperature, the integration time constant of operation, and the intensity and energy of the incident radiation. The calibration tests at Goddard Space Flight Center were performed at ambient temperature. These tests, presented in figure 3.4, demonstrated a linear dependency of the IES pedestal centroid position upon the intensity and energy of the incident mono-energetic particle beam. This allows us to model the pedestal centroid position as a function of all these dependencies with a best fit linearized model of the form $y = m \bullet x + b$. The slope, m, represents the instrument response to it's environment, and is extracted from calibrations performed at Goddard Space Flight Center. The combined effect of the intensity and energy of the incident mono-energetic particle beam upon the measured pedestal centroid position is accounted for by having x represent the mono-energetic particle beam intensity multiplied by it's energy. The pedestal response of the IES to no incident radiation is then accounted for by having b represent the pedestal centroid position when x is zero. The result, y, is then the predicted pedestal centroid position.

Figure 5.1 illustrates the measured pedestal position as a function of intensity (kHz) and energy (keV) for look direction 5 at 2 μs, 10 μs, and 100 μs time constants. A best fit linear model to the measured pedestal position yields the following sets of equations:

$$P_{2\mu s} = -0.00065967(I \bullet E) + P_m$$
$$P_{10\mu s} = -0.0040365(I \bullet E) + P_m$$
$$P_{100\mu s} = -0.0413240(I \bullet E) + P_m$$

Where I is the incident particle intensity in kHz, E is the incident particle intensity in keV, and P_m is the measured pedestal position of the IES with no incident radiation, performed at ambient temperature.

The slope from the above equations is plotted in figure 5.2 as a function of integration time constant, and is depicted to have a linear relationship. Generating a best fit linearized model for the slope yields $Slope = -0.00041468 \bullet X_{ITC} + 0.00014125$, where X_{ITC} is the operational integration time constant. Substituting *Slope* into the linearized model for the pedestal position yields the following equation for a calculated pedestal position as a function of the integration time constant and the incident mono-energetic particle beam intensity and energy:

$$P_d = = (-0.00041468 \bullet X_{ITC} + 0.00014125)(I \bullet E) + P_m$$

The predicted pedestal position, P_d, is plotted beside the measured pedestal position in figures 5.3, 5.4, and 5.5 for the 2 μs, 10 μs, and 100 μs integration time constants respectively. The results illustrate a good prediction of the instrument response to its particle environment and operating parameters.

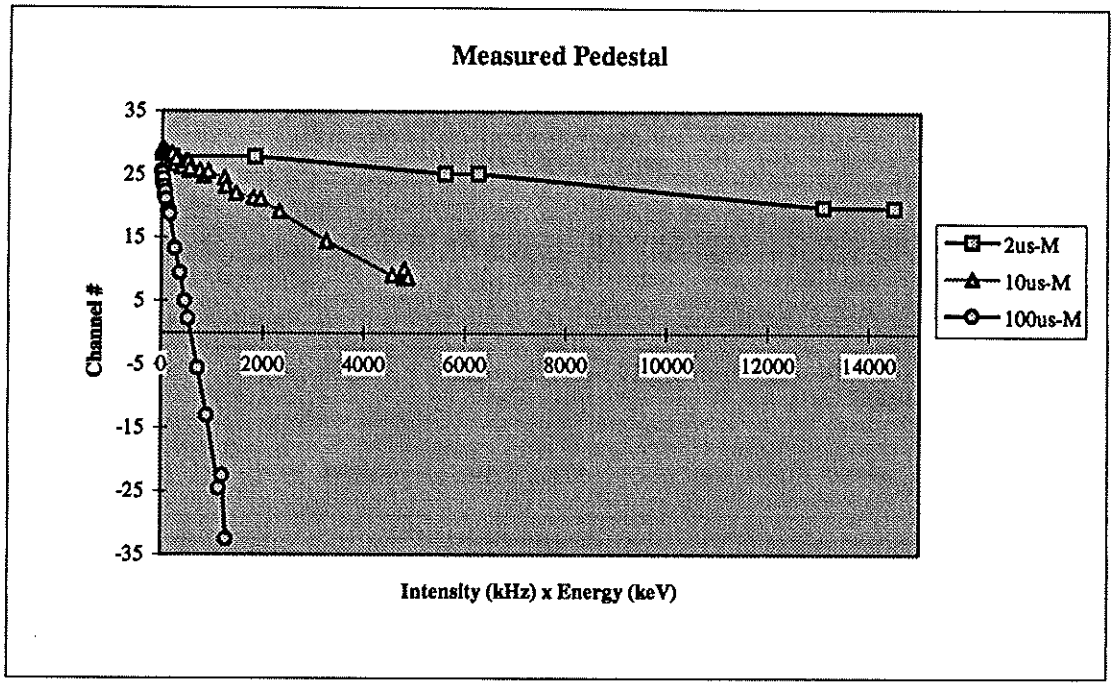

Figure 5.1: Measured pedestal for 2 us, 10 us, and 100 us time constants.

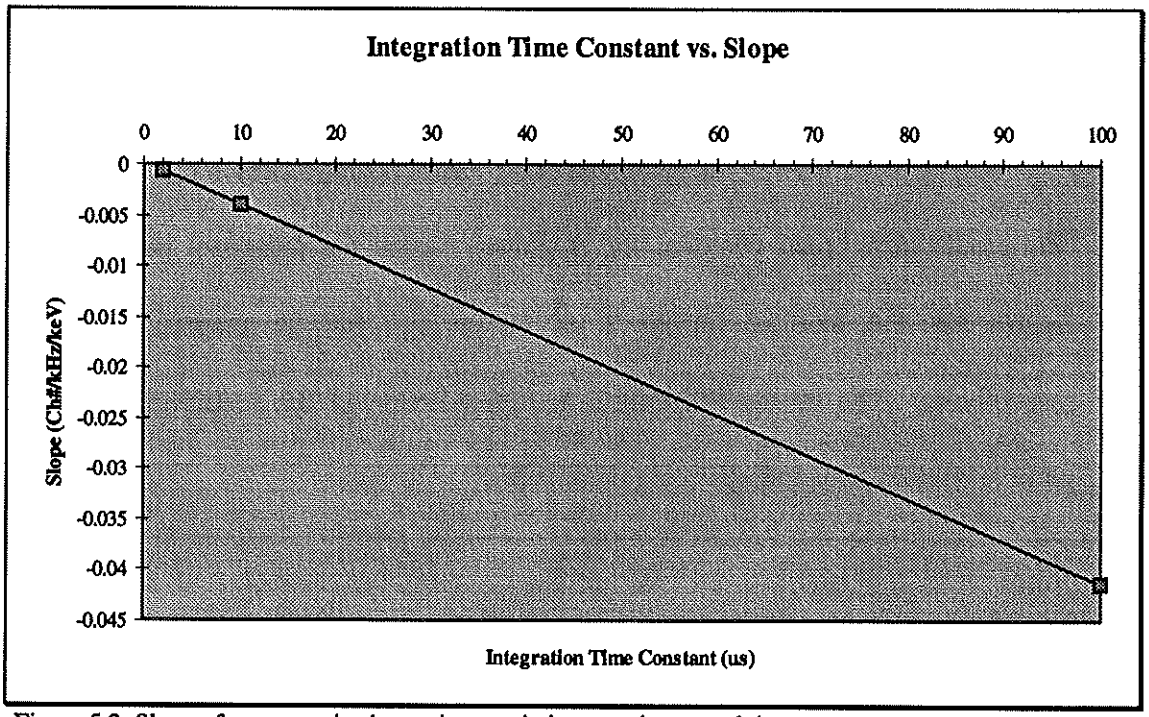

Figure 5.2: Slope of parameterized equations variation over integrated time constants.

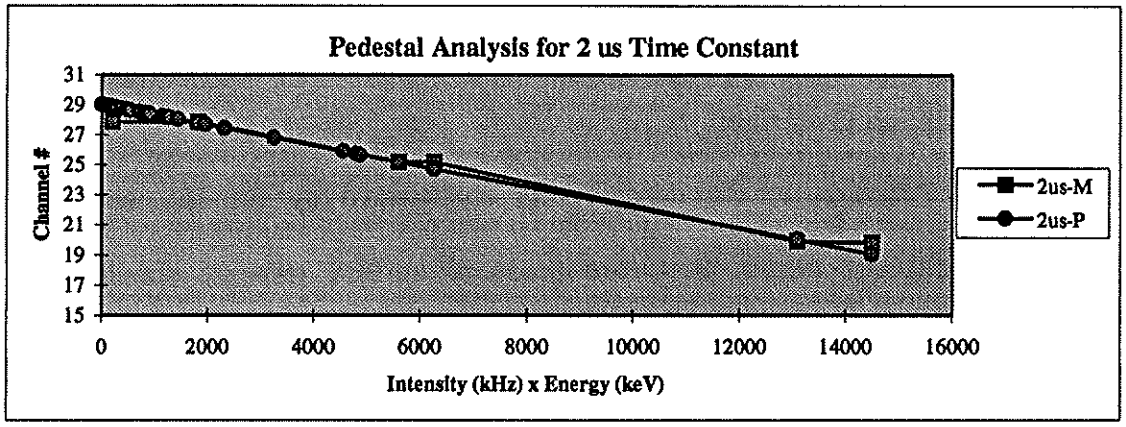

Figure 5.3: Measured pedestal vs. Parameterized pedestal for 2 us integration time constant.

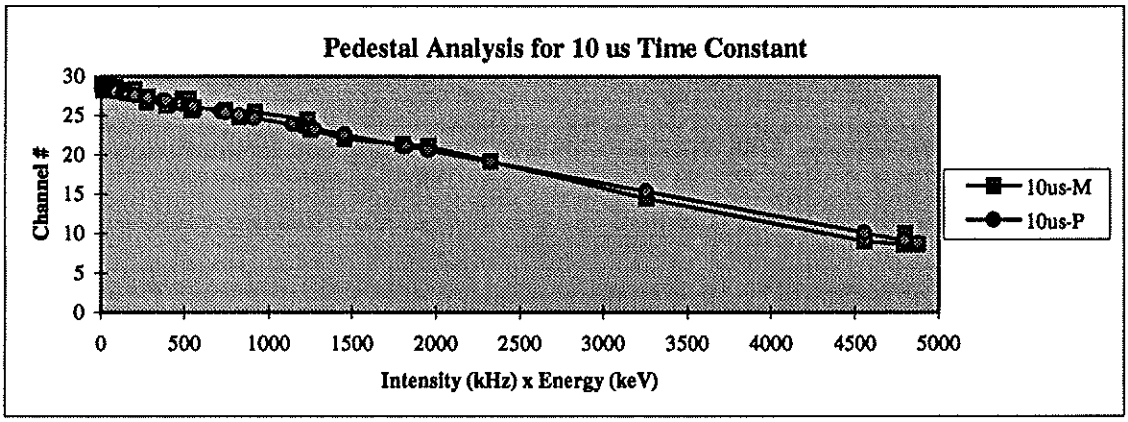

Figure 5.4: Measured pedestal vs. Parameterized pedestal for 10 us integration time constant.

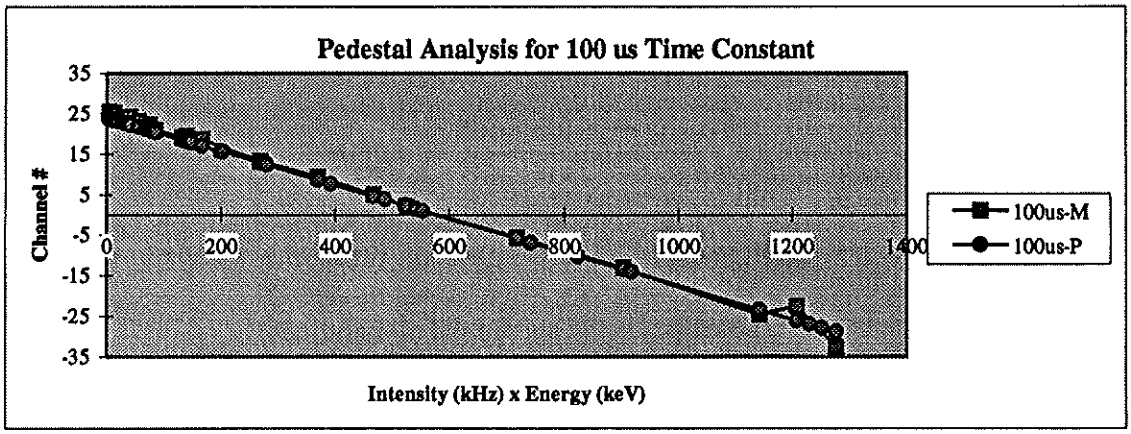

Figure 5.5: Measured pedestal vs. Parameterized pedestal for 100 us integration time constant.

Chapter Six

IES Simulation

6.1 Simulation Overview

In response to the dependencies encountered by the IES on its operating environment and modes, RAL had produced an IES response simulation package, performed in IDL code, to account for the instrument performance. Figure 6.1 illustrates the command module for the simulation software. The following describes the input parameters, labeled in figure 6.1, required by the simulation (Perry, 1996):

1. Integration Time (μs) - The integration time constant selected for instrument operation. This represents the live time during one accumulation cycle.
2. Pedestal Width (Channel #) - The sigma ($\sigma = FWHM/2.35$) of the pedestal with no radiation incident on the instrument.
3. Binning Interval (sec.) - This parameter reflects the time period for which the simulation will run, and may be selected to range between 0.01 to 10.0 sec.
4. Number of events (1/sec.) - Denotes the intensity seen by the instrument. The total events is represented by the number of events multiplied by the binning interval.
5. Number of Iterations - The number of times the software will repeat the simulation. The output is the average of all iterations.

6. Readout time (μs) - The dead time for the IES during one accumulation cycle. This value has been analyzed to be 48 μs for IES #6.
7. AC time constant (μs) - Time constant of the exponential decay associated with the AC coupling of the sensor.
8. AC accuracy (≤1.0) - Threshold for return current, modeled by the exponential decay associated with the AC time constant in 7.
9. Pedestal Position (Channel #) - The pedestal centroid position as recorded with no incident radiation.
10. Input Electron Distribution- File in simulation directory which consists of the distribution of the incident radiation which is desired to simulate the instrument response. File should consist of two columns, one for channel number, and one for the associated counts.
11. Binning Table - File in simulation directory which consists of the energy binning of the resultant output.
12. Results Save File - File in simulation directory which consists of the resultant output from simulation.

The simulation converts the input electron distribution (10) into a normalized probability distribution of the form $P(x) = \frac{\sum_{i=0}^{x} f(i)}{\sum_{all\ i} f(i)}$. In order to associate a time with the event, a random number list, $R_1(n)$, is generated where n represents the total number of

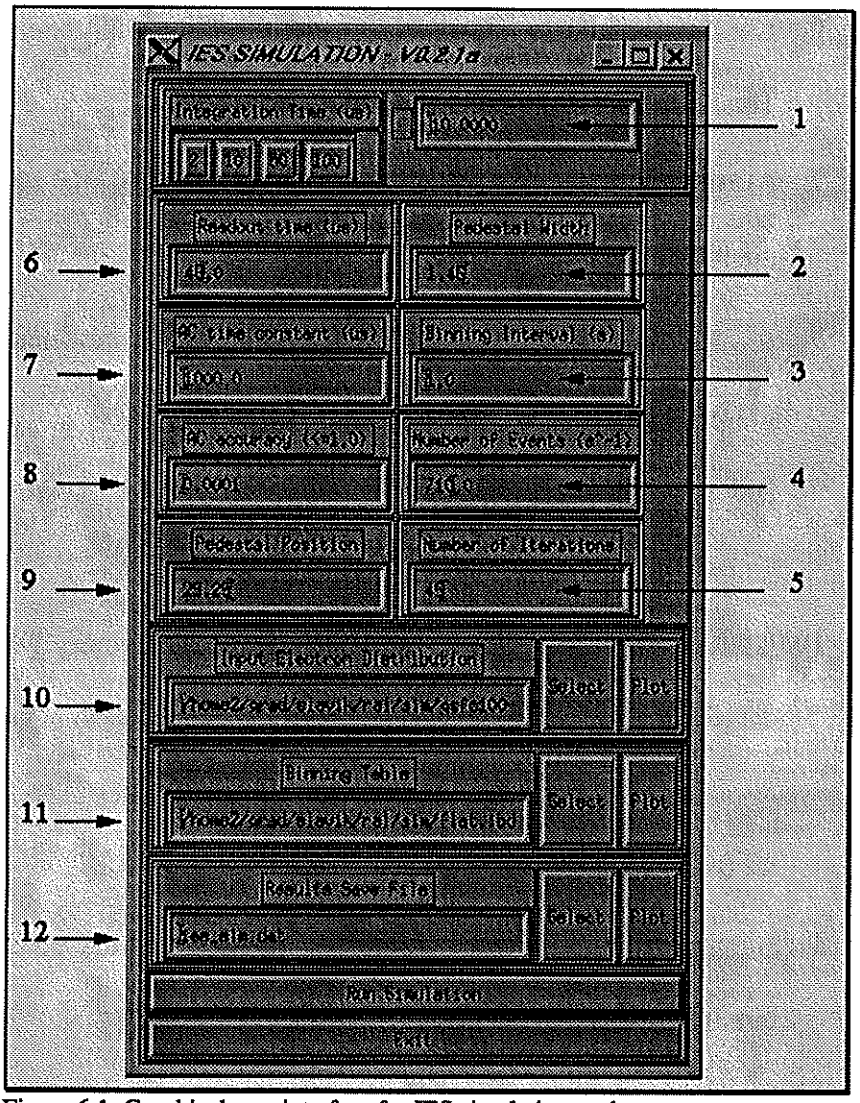

Figure 6.1: Graphical user interface for IES simulation package.

events during the simulation. The time associated with the event is then calculated to be $t(n) = t_{start} + (t_{end} - t_{start})R_1(n)$. A second list of random numbers, ranging between 0 and 1, is then generated to associate an amplitude with the event. The random number generated is converted into an energy provided. A time line is generated over the binning interval,

and the time of the event is then determined with respect to the time line. Should the event fall within the integration period, its contribution is the difference between the positive current of the signal to the negative current associated with the return to baseline signal, as illustrated in figure 3.5. However, should the event fall during the dead time period, the return to baseline current effect is subtracted from the following integration period. The return to baseline current continues to effect subsequent integration periods until its value falls below the AC accuracy (8). Pile-up is simulated when two events obtain a random time number associated with the same integration time period. The pedestal is then introduced by randomly selecting from a gaussian distribution, and by the input parameters given in 2 and 9 above. It's shifting effect is simulated through the negative effect of having an integral return signal greater than an integral signal for a specific integration period (Perry, 1996).

6.2 IES# 6 Simulation

Simulation of IES# 6, at 10 μs integration time for look direction 5, was performed. Figures 6.2 and 6.3 illustrate the input electron distribution and the resultant probability distribution. The simulations were run with a 1 second binning interval and 45 iterations. The pedestal was determined to be at channel 29.25 with a sigma of 1.46. A 48 μs dead time was chosen with an AC time constant and AC accuracy left in their default values, 1000 μs and 0.0001 respectively. The flat energy binning scheme was selected for a linear energy scale. For the various intensity simulations, only the relative intensity was altered.

Figures 6.4 to 6.10 illustrate the simulated IES response to the intensity provided in table 3.2 for look direction 5, 10 μs integration time, with a 100 keV mono-energetic beam incident on the instrument. The results illustrate a good understanding of the IES response to a known input electron distribution.

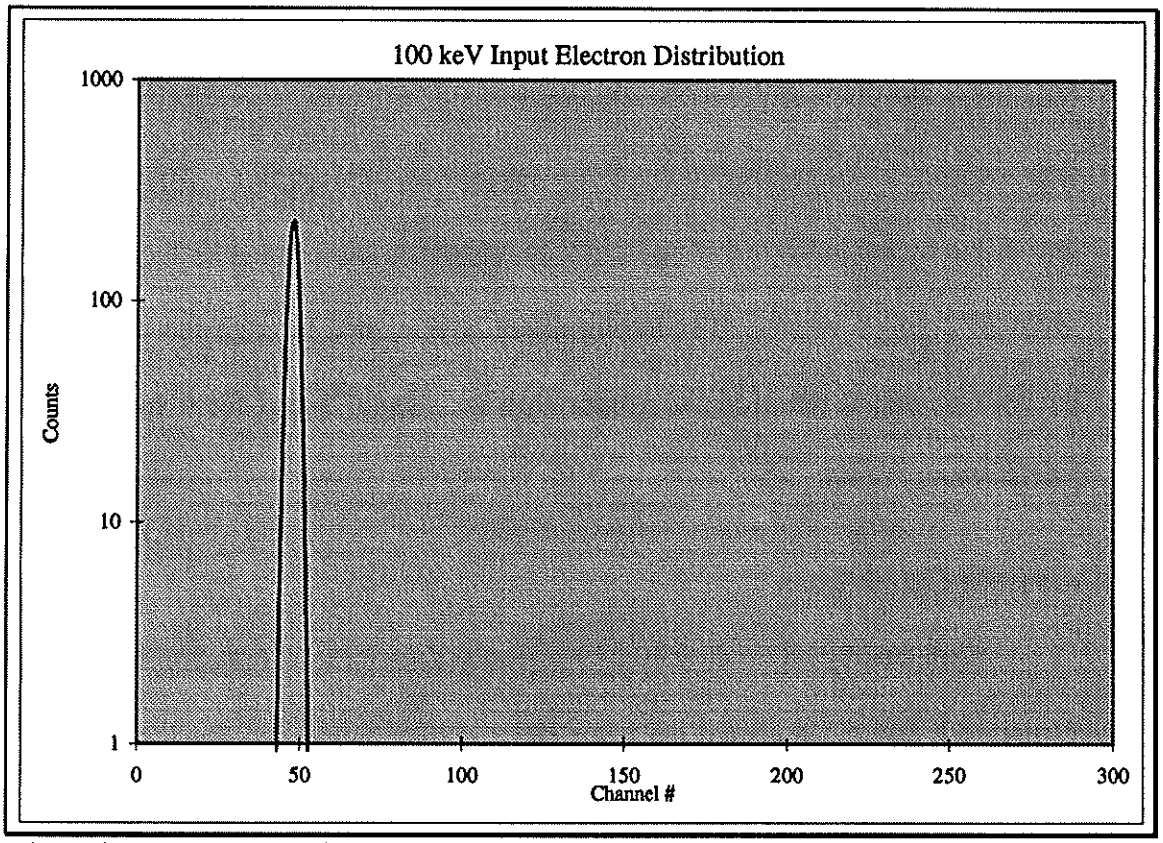

Figure 6.2: Input electron distribution for a 100 keV particle beam given as an input to the RAL IES simulation.

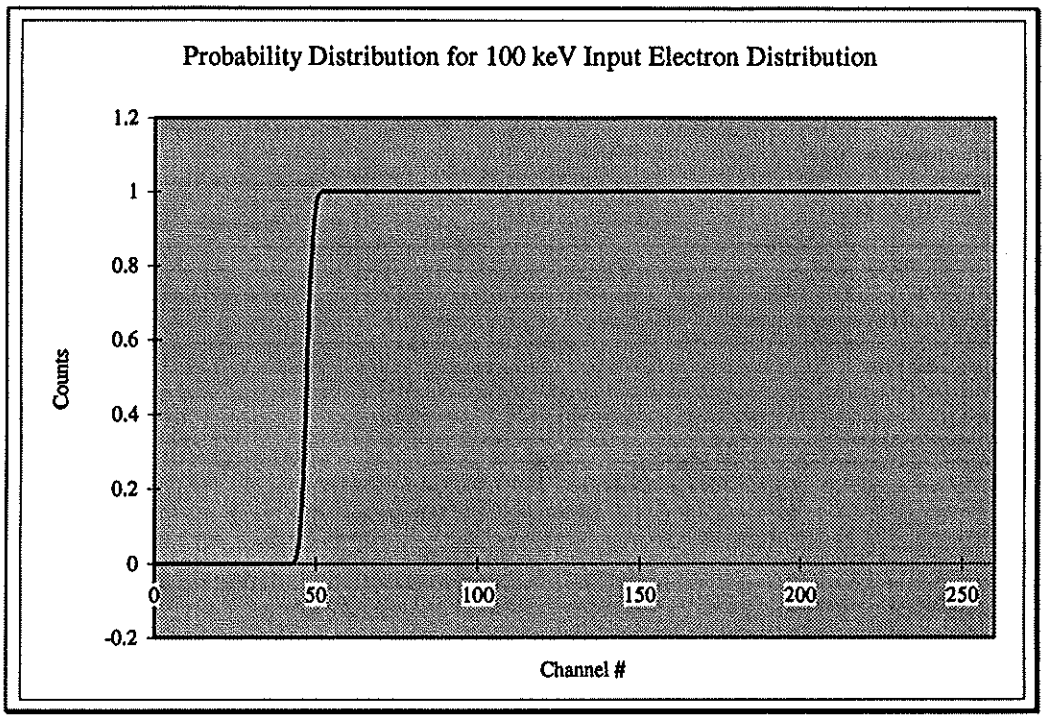

Figure 6.3: Probability distribution for 100 keV input electron distribution.

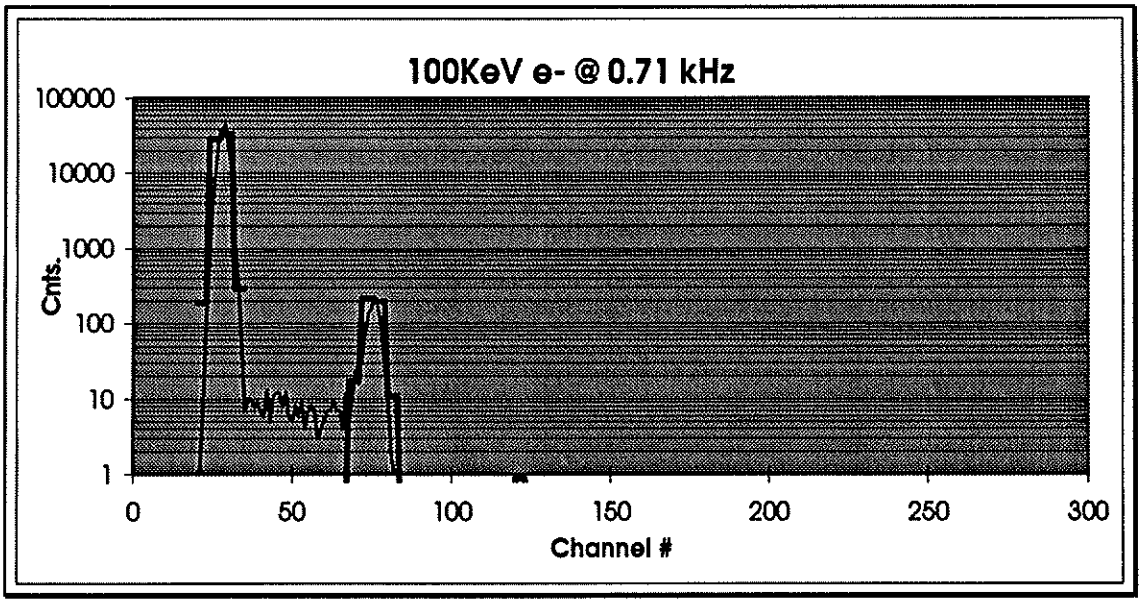

Figure 6.4: Simulated (dark) vs. Measured spectrum at 0.71 kHz intensity.

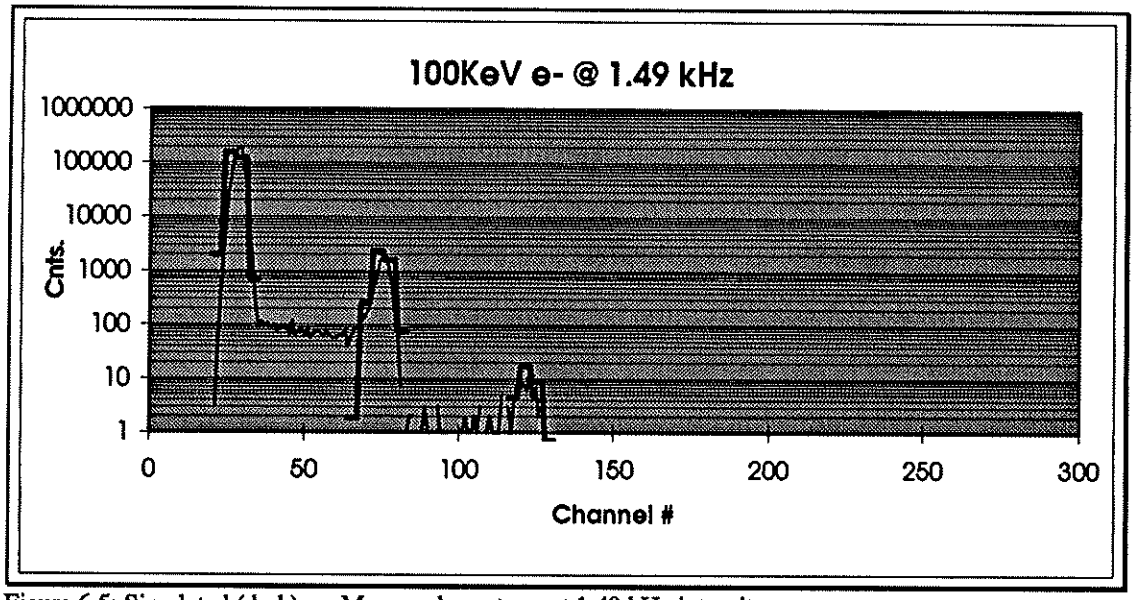

Figure 6.5: Simulated (dark) vs. Measured spectrum at 1.49 kHz intensity.

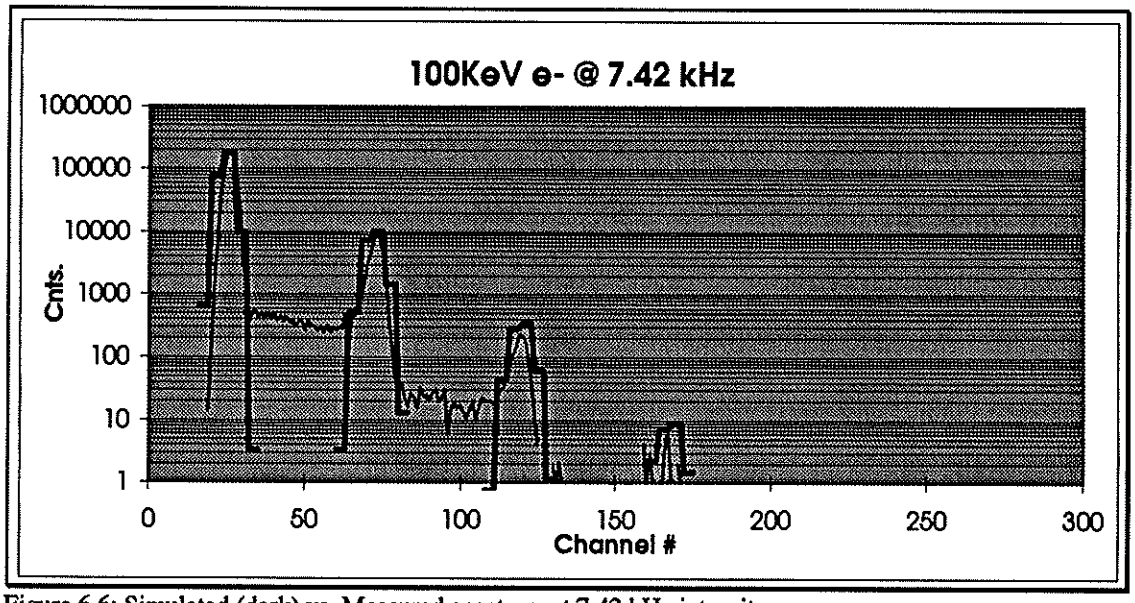

Figure 6.6: Simulated (dark) vs. Measured spectrum at 7.42 kHz intensity.

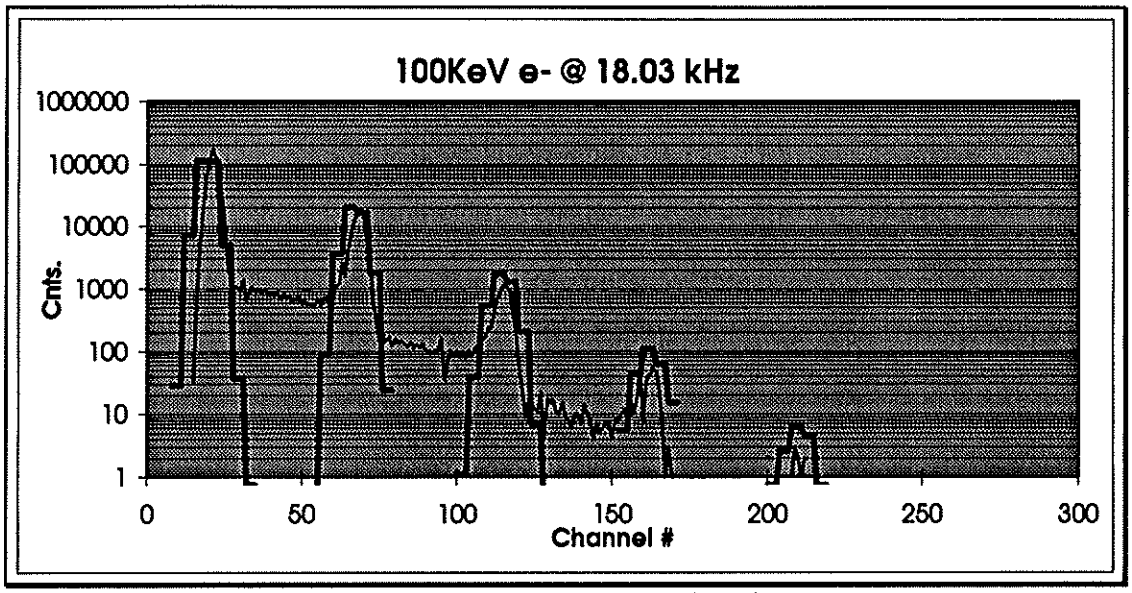

Figure 6.7: Simulated (dark) vs. Measured spectrum at 18.03 kHz intensity.

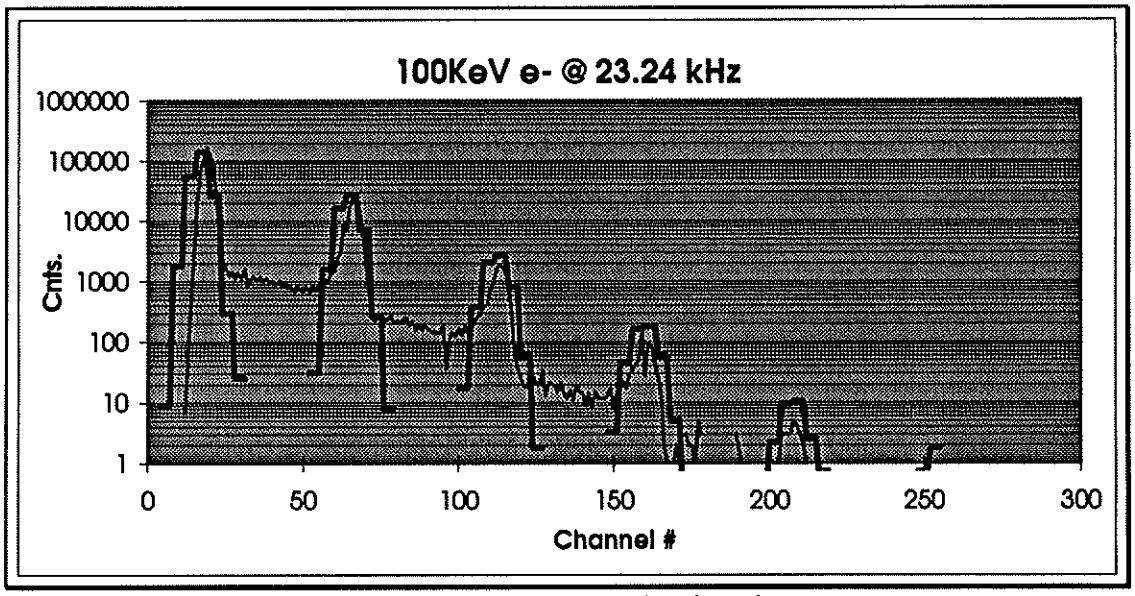

Figure 6.8: Simulated (dark) vs. Measured spectrum at 23.24 kHz intensity.

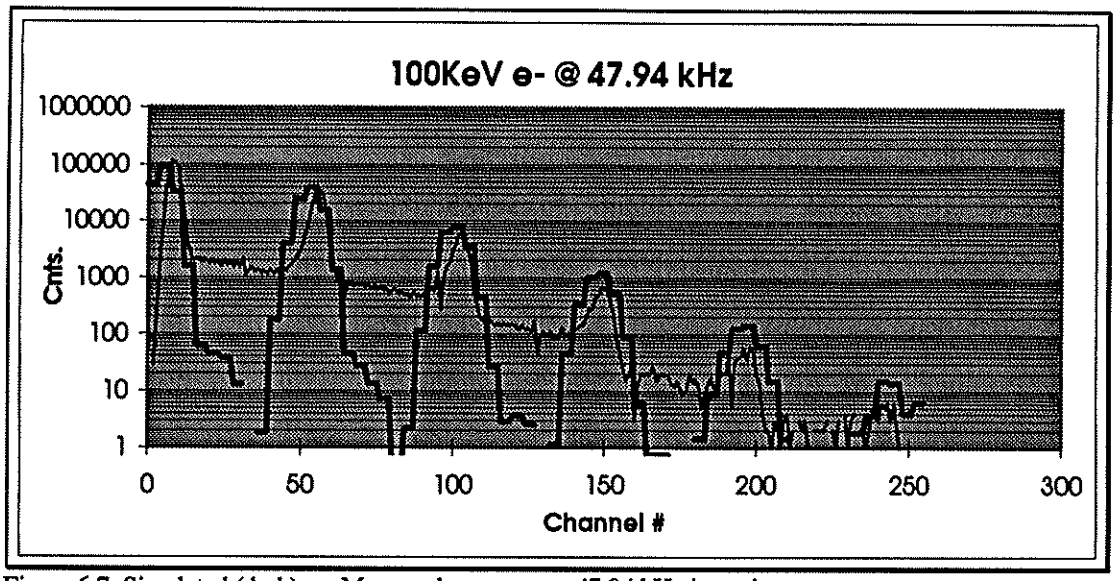

Figure 6.7: Simulated (dark) vs. Measured spectrum at 47.94 kHz intensity.

Conclusion

The IES represents an instrument utilizing solid state device technology capable of performing high resolution energetic particle measurements. This represents a promising technology for the fabrication of small, light weight systems with the ability to out perform conventional spacecraft instrumentation. However, testing of the IES has revealed a need for a better understanding of the various operational aspects of this system.

The IES has presented a number of unexpected system responses to its operational mode and environment. The instrument baseline and noise response has been demonstrated to fluctuate with the integration time constant of operation, the instrument temperature, the intensity and energy of the incident radiation, and the look direction which is of interest. Calibration of the IES has been performed to compensate for the effects of the numerous dependencies of the instrument, and to better understand the data returned.

Characterization of the IES with calibrations performed at Goddard Space Flight Center has been performed, and has proven a high level of understanding of the instruments' performance. Comparison of the parameterization equations and measured instrument performance has been illustrated to show a good correlation. Also, simulation software for the IES, produced by RAL, has been demonstrated to have a good understanding of the instrument performance. It has been illustrated that with the present understanding of the IES, reliable measurement can be extracted and accurately interpreted from data returned from orbit.

APPENDIX I: Goddard Space Flight Center Calibrations

June 26-30, 1995 - The IES sensor head incorporated with the CEPPAD stack was taken to Goddard Space Flight Center for angular efficiency tests. The unit was supported with the Hugins chip and electronics prepared by Geri Levine. Support for these calibrations were provided from Boston University, Center for Space Physics by Prof. Theodore Fritz, Ms. Gina Gugliotti, Ms. Dimple Patel, and by the author. On June 29th the IES noise response had increased. During the examination of the unit improper biasing was applied, and resulted in a total systems failure. It had been decided that this was unrecoverable, and to end the calibrations for unit refurbishment at a later date.

August 21-25, 1995 - The IES sensor head incorporated with the CEPPAD stack had been refurbished due to a system failure which occurred during the June 1995 calibrations. The unit had been taken down to Goddard Space Flight Center for further angular efficiency tests. Support for these calibrations were provided from Boston University, Center for Space Physics by Prof. Theodore Fritz, and the author.

January 18-23, 1996 - IES# 4 had been tested utilizing Steve Brown's facility at Goddard Space Flight Center. Berend Wilken, Wolfgang Gutler, & Reiner Rathje provided support from Germany for the testing as well as the ground support equipment to the unit (flight DPU and GSE). Rob Sheldon and the author had provided support from Boston University. The testing included:

- Europium calibration.

- Electron data runs over various intensities, energy, and look directions.
- Ion data runs over various intensities, energies, and angles.

The intensities for the electron data runs ranged from 100 Hz to 100 kHz using 200 and 400 keV electrons. All of the histogram mode data was taken at 10 μs integration time. Look direction 5 was the primary source of testing, while look directions 4 & 6 had data runs for 2 different intensities. Steve Brown's Van de Graff machine was used for these tests, and all of the electron intensity testing was completed on Monday Jan 20th, 1996.

The following is a summation of the data analysis meeting held concerning the electron intensity testing of the Rapid IES flight spare to be flown on CLUSTER:

1. In all instances within the data set, there is a pedestal dependency on the electron intensity rate incident on the unit at 200 keV and 400 keV. The incident intensity had been measured with a reading over a calculated area of a detector monitor before and after a data run. As the monitor rate increased, the pedestal appears to shift down the spectrum, and eventually shifts off the spectrum range and is binned into channel 0. The intensities had ranged from 100 Hz to 100 kHz. It is worth noting that with exceptions, the total counts recorded for a data run (Pedestal + (Pedestal + Signal)) remained relatively consistent. An increase in intensities decreased total pedestal counts, but increased pedestal + signal counts to maintain a steady value for the total counts accumulated throughout the spectrum.

2. The gain of the system is relatively constant despite the shift in pedestal. Gain fluctuates about the 1.9 keV/Ch# margin with about a ±0.1 keV/Ch#.
3. A peak broadening has been observed with increasing intensities. This is believed to be the functionality inherent in the electronics of the RAL chip, but appears as though requires a more comprehensive investigation to be able to understand this effect electronically. As intensities increase beyond 10 kHz for 400 keV, and 3 kHz for 200 keV, a relatively flat spectrum is observed with no distinguishable energy peaks.
4. An observation during a data run of 1.6 MeV protons at 10 μs integration time produced a blank spectrum of the incident look direction 5, but also affected its adjacent look directions 4 & 6 in the same manner...it is noted that no pedestal was recorded in either of the three look directions. However, at a 2 μs integration time of 1.6 MeV protons, the pedestal was accumulated in all three look directions. It was suggested by Berend Wilken at the time of the data run that this could be a result of saturating the amplifier in the RAL chip.
5. Pile up was noticed for the 200 keV electrons at all the intensities which produced a distinguishable spectrum. The pile up of the 400 keV runs were only noticeable when a high enough intensity was used to shift the spectrum adequately enough to be able to distinguish a 2-pulse pile up. Pile up has been recorded to be nominally 10% of original energy distribution, but requires a further detailed analysis at this point. Low energy

runs of 30, 40, and 60 keV electrons produced a spectrum containing up to a 3-pulse pile up, but again requires further analysis.

September 30 - October 4, 1996 - IES # 6 had been taken down to Goddard Space Flight Center for further IES intensity and energy calibrations utilizing Steve Brown's facility. Support for the calibrations were provided from Boston University by Dr. Rob Sheldon, Dr. David Matthews, and the author, and from Los Alamos National Laboratory by Mr. Roy Cope. The testing had produced calibrations of the IES# 6 for all measurable intensities and energies, and has been utilized for the understanding provided in this document. A full inventory of the calibrations performed is given in table 3.2.

APPENDIX II: Integrated Systems Tests of IES

Integrated System Tests were performed on IES# 1, 2, 4, 5, and 6 at Centre National d'Etudes Spatiales in Kourou, French Guiana. Along with support from MPAe and IDA, support for the IST's were also provided from Boston University by Prof. Theodore Fritz, Mr. Anders Jorgensen, and the author. Previously, the IES had only been tested in Germany utilizing the 2 μs integration time. The IST's represented a full, end to end test of the IES while integrated onto the Cluster satellites. Initially, the IST's were to be performed solely for the 2 μs integration time. However, during the IST for IES# 1, it was discovered that high frequency noise was severely affecting the longer integration time periods as discussed in section 4.3. A revised IST format was then introduced to analyze all integration time constants, and the IST for IES# 1 was then to be redone. The new format of the IST's were such that the center look directions, and the 2 μs integration time constant were interrogated for the longest period of time. The following is an example of an IST:

Look Direction	IST Accumulation Periods			
	2 μs	10 μs	50 μs	100 μs
1	7 minutes	2 frames	2 frames	2 frames
2	7 minutes	6 minutes	6 minutes	6 minutes
3	7 minutes	2 frames	2 frames	2 frames
4	7 minutes	2 frames	2 frames	2 frames
5	7 minutes	6 minutes	6 minutes	6 minutes
6	7 minutes	2 frames	2 frames	2 frames
7	7 minutes	2 frames	2 frames	2 frames
8	7 minutes	6 minutes	6 minutes	6 minutes
9	7 minutes	2 frames	2 frames	2 frames

The time line for the IST's performed on the Cluster/RAPID units and the associated support from Boston University are the following:

Flight Unit No.	IES No.	IST Date (MM/DD/YY)	Supported by
1	6	09/27/95	Mr. Anders Jorgensen
2	1	09/11/95, 02/17/96	Prof. Theodore Fritz, Author
3	2	10/12/95	Author
4	5	09/28/95	Mr. Anders Jorgensen
5	4	02/19/96	Author

The IST's had revealed that IES# 6 maintained a higher noise degradation over the other units, and was decided to be replaced with IES# 4 on February 19, 1996.

APPENDIX III: RAL Simulation Software Users Guide

RAL CEPPAD IES SIMULATION SOFTWARE
v0.2.1 Alpha

Users Guide

Release - Draft 0.1

C.H.Perry@rl.ac.uk

1. Introduction

This simulation is designed to help investigate the effect of electron count rate and distribution on the measured IES output. The model is simple but accounts for the three main instrumental factors that affect the measurements, namely:-

- AC coupling of the detector
- Duty Cycle
- Pile Up.

This document is intended as an overview to the operation and use of the of the IES simulation software.

2. Simulation Overview

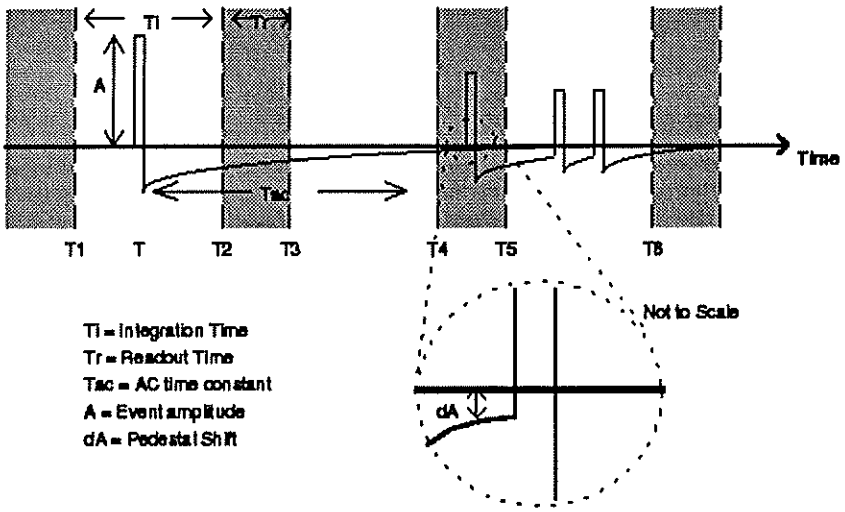

Figure 1 Simplified view of IES response to events. The shaded regions represent readout periods during which the signal is not integrated. The solid line indicates the input signal. The expanded region shows the shift in the baseline (dA) just before an event.

2.1 AC Coupling

The two main timing periods are Ti, the integration time and Tr, the readout time. Events that occur during the integration period (e.g. the event between T1 and T2) have a certain amplitude, A. Since the sensor is AC coupled, over a period of time, there must be an equivalent return signal. This is expressed by an exponential decay with time constant T_{AC}. T_{AC} is typically much longer than the integration time and therefore the effect of the return signal on an individual sample period is small compared to the event amplitude.

The measured signal obtained for a particular sample period is the combination of the event signal and the return signal (which is of the opposite sign). For example, the level detected between T1 and T2 (Figure 1) is the combination of the signal due to, A, and the return signal between T and T2. In

this case the contribution of the return signal depends on the position of the event within the sample period. The observed effect is to drive down the apparent measurement baseline resulting in an under estimate of the actual event amplitude by dA.

To minimize the impact of this effect, the integration time should be kept as short as possible relative to the decay time, T_{BC}. Ideally T_{BC} should be large enough to spread the return signal over as long an interval as possible thus minimizing the impact on any individual sample period. This only remains true while T_{BC} remains shorter than the average time between events. As the event rate rises above this level the return signal from near-by events become super imposed. For a constant high event rate the result is a uniform shift of the measurement baseline for all events. Under more realistic conditions neither the count rate or the incident electron spectrum will remain constant. It is therefore useful to remember that the centroid of the measured distribution is constant and co-located with the mean pedestal energy at low (zero) count rates. Determination of the pedestal shift at higher count rates can be used to calculate the mean energy shift of the measured spectrum.

The situation is further complicated by the binning of the data since this imposes restrictions on how accurately it is possible to determine the shift. At high count rates the shift in the baseline can result in such a large shift that signals fall below the nominal threshold of the lowest ADC bin. In such cases the event will be assigned to the lowest bin thus overestimating the true signal level and resulting in an underestimate in the baseline offset. This will also exhibit itself as an upward shift in the calculated centroid position. A similar situation can occur at the high energy end of the scale resulting in a downward shift in the centroid position. At very high count rates the combination of these two effects, together with pile up of multiple events make it virtually impossible to determine the true input population.

2.2 Duty Cycle

Events that occur during the readout time (e.g. the event between T4 and T5) will not be recorded by the system. Therefore T_r represents the dead time of the system and the observed count rate should be corrected by the factor $(T_i+T_r)/T_i$. To minimize the impact of the duty cycle on the system the ratio of T_i/T_r should be made as large as possible. Note that although the event is not recorded the AC coupling effect described above must still be accounted for.

2.3 Pile-Up

Since the IES is sample and not event driven two or more events that occur within the same integration period (e.g. the events between T5 and T6) will be recorded as a single larger event. To avoid event pile-up T_i must be set sufficiently low that the probability of receiving more than one event during an integration period is small. Typically T_i should be set to $\leq$ 10% of the mean event rate.

Pile up correction = TBC

3. Simulation operation

The software consists of two parts, 1) The IES event simulation and 2) The results plotter. These communicate with each other via a results file than contains a set of data stored in IDL "SAVE" format.

3.1 IES event simulation

The simulation takes the input electron distribution and generates a normalized, integral probability distribution:-

$$P(i) = Sum(f(j),j=1,i) / Sum(f())$$

The value P(i) represents the probability of an event in or below channel "i" and will varies from a value of 0 at the lowest channel up to 1 at the maximum channel. To generate the list of events used by the simulation two sets of uniform random numbers are generated. The first set is used to produce the event timing where $t(n) = tstart + (tend-tstart)*R_1(n)$. The second set are used with the probability distribution to generate an event amplitudes (channel numbers) using $a(n) = P^{-1}(R_2(n))$. Where P^{-1} is the inverse of the probability function described above.

A time line is initialized corresponding to the individual sample periods (Ti+Tr) within the simulation period Tp. The number of sample periods is just Tp/(Ti+Tr). For each event the sample period in which it falls is determined. If the event falls within the integration part of the sample period its amplitude is added to the current sample. The AC coupling of the sensor is modeled with an exponential decay with time constant, τ, where the integral is equal to the event amplitude. For events falling within the integration part of the sample period, the return current between the event time and the end of that integration is subtracted from the sample. Events occurring during the readout time have no effect on that sample period. For subsequent periods the return current during Ti is calculated and subtracted from the sample accumulation. This is continued until the return current level falls below a threshold defined by the simulation accuracy. Multiple events falling within the same sample period are summed together to simulate the effect of pile-up.

Once all events have been processed a pedestal signal is added to each sample. The pedestal signal is randomly selected from a Gaussian distribution with user defined position and width. The final accumulated signal in each sample period is binned to generate the output distribution. The histogram procedure uses a binning table allowing the bin thresholds to be set to match those of the instrument. If multiple iterations have been requested the above procedure is repeated and the average of the final distributions calculated. On completion, the simulation corrects the resulting distribution for the sample period duty cycle and outputs the input, output and event information to the results file.

3.2 Results Plotter

The results plotter reads the output file and displays the input distribution (dashed line), output distribution (solid line) and shows the location of the unshifted pedestal (dash-dot line). The triangular markers on the top and bottom axis indicate the calculated centroid of the distribution which for low count rates should be coincident with the unshifted pedestal position. The lower panel displays a time slice of sample accumulations (solid line) together with individual events (crosses). Events that fall during the readout period are plotted with negative amplitudes to distinguish them from those that are directly accumulated. A horizontal dotted line is used to show the position of the unshifted pedestal.

4. Quick Guide to using the IES simulation

Change to the directory that contains the simulation software and start IDL.

At the IDL prompt type :-

```
IDL> @run_sim
```

4.1 Using the Simulation

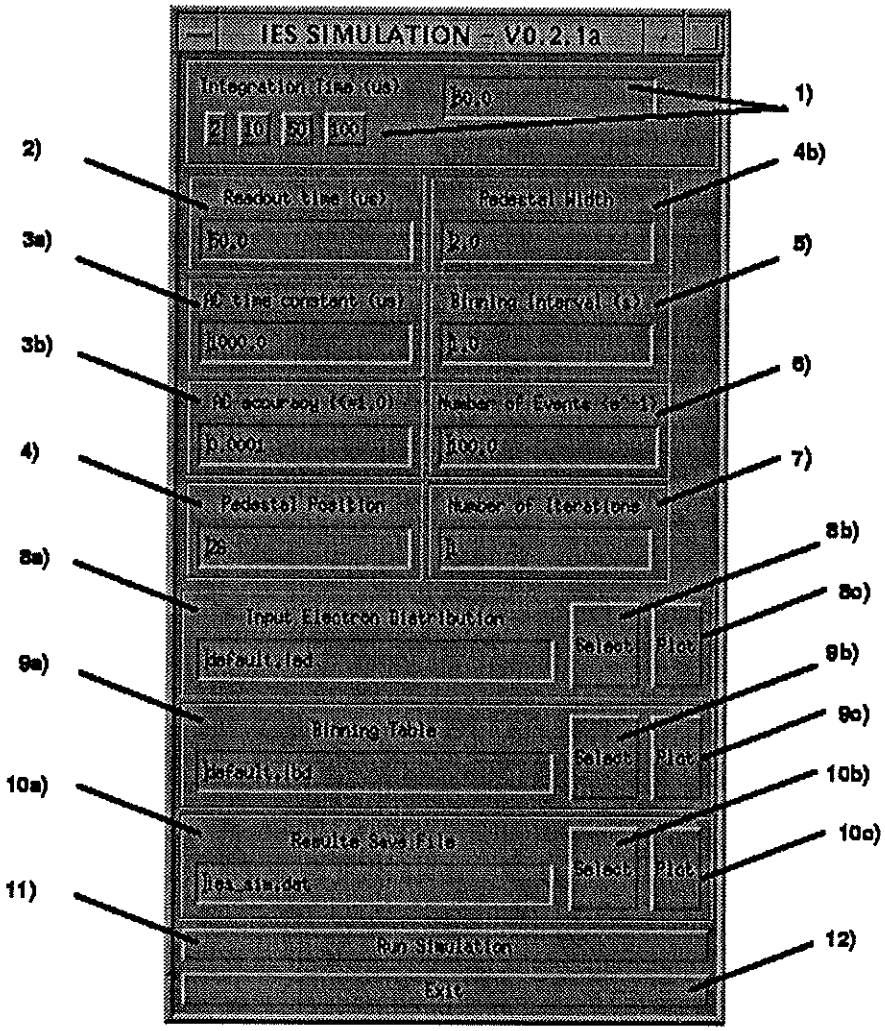

The main IES simulation control panel. The numbered controls are described in the text

Once the simulation has started the display shown in Figure 2 should appear.

1) Integration time. The part of a sampling interval during which events are recorded. The length of one sample period is the sum of the integration time and the readout time.

2) Readout time. The part of the sampling period during which the signals are being read by the DPU and therefore the detector is in-sensitive to new events. Events that occur during the readout time may still have an effect on subsequent sample periods due to the AC coupling of the sensor.
3) AC Time Constant. This defines the time scale over which the AC coupling operates.
4) Pedestal Position. The central (mean) channel number of the unshifted pedestal.
4b) Pedestal Width. The half-width at half-amplitude (TBC) of the Gaussian pedestal distribution.
5) Binning Interval. The time for which the simulation will be run (0.01 to 10.0s).
6) Number of events. This specifies the count rate (number of events per second) used by the simulation. The total number of events processed by the simulation per iteration is this value multiplied by the binning interval. The distribution of these events is dictated by the input distribution function (see 8).
7) Number of Iterations. The number of iterations to be completed. The resultant output distribution from all the iterations are averaged to generate the final result. The event information contained in the output file comes from the last iteration.

8) Input Distribution. File from which the input electron distribution is read. This data is used to build the event list and should consist of two columns containing the channel number (can be fractional) and the relative level.
9) Binning Table. File from which the binning information is read. The file contains two columns containing the bin number (integer starting at zero) and the corresponding ADC channel number. Events with an ADC outside the bin range are placed in the lowest/highest bin accordingly.
10) Results File. The file to which the output spectrum is written. The current selection is shown in the text field. This can be modified or the **Select** (10b) button can be used to bring up a file requester from which an existing file can be picked. The **Plot** (10c) button brings up the plot interface that reads the results file (see below).
11) Run the Simulation.
12) Exit the simulation. This will close the simulation interface. If the plot interface is running this must also be closed before the IDL prompt will appear.

Notes
Readout time, AC time constant and Accuracy can probably be left at their default values.

The simulation is slow so its best to do a quick run using small binning intervals and low number of iterations first, then increase them to improve the statistics once the other parameters are correctly set. Increasing the binning interval is more costly in terms of processing power and memory but you may not have a choice when looking at low rates.

Changes can't be made once the simulation has started and the only way to stop it prematurely is to <CTRL C> from the IDL command line.

4.2 Using the Result Plotter

Once the simulation has completed, the results can be plotted using **Plot** button next to the **Results Save file** entry. If there is a valid results file this will bring up the plot interface:-

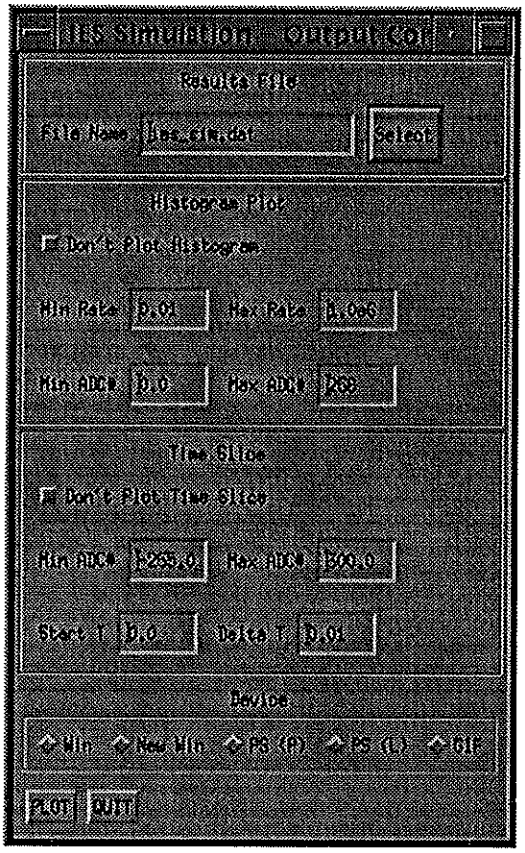

This will be set to the same value as on the main control interface and should only need to be changed to load a previously stored result.

The **Histogram Plot** displays the simulated spectrum. For comparison, the input spectrum and pedestal are also displayed.

Y and X axis limits can be changed using these controls or the whole panel disabled.

The **Time Slice** plot displays the content of the individual sample periods. The input events are overlaid as a reference. Events that lie during the readout period are set to a negative value.

The Y axis limits and the slice position and width can be changed using these controls or the whole panel disabled.

Use these 'radio' buttons to select the output device.

Select **Plot** to plot or **Quit** to quit.

The default device, **Win**, outputs to the current window, **New Win**, creates a new window, **PS** produces **(P)**ortrait or **(L)**andscape output in the default IDL output file (idl.ps). **GIF** generates a GIF file called idl_###.gif where ### is a sequence number starting at 000.

The input file is re-read each time a plot is requested so there is no need to quit and re-enter each time a new simulation is complete. If you try to plot while the simulation is busy nothing will happen until the simulation is complete.

BIBLIOGRAPHY

Blake, J. B., *et al.*, 'CEPPAD. Comprehensive Energetic Particle and Pitch Angle Distribution Experiment on POLAR', *Space Sci. Rev.*, **71:** 531-562, 1995.

Carter, M., 'Polar Results', ftp://shaper.bnsc.rl.ac.uk/pub/POLAR/CEPPAD/RESULTS/, 1996.

Contos, A. R., 'Complete Description and Characterization of the High Sensitivity Telescope (HIST) Onboard the Polar Satellite', *Master's Thesis*,1997.

Henderson, M. G., 'Sector Cartoon', http://nis-www.lanl.gov/~mgh/ENA.shtml, 1996.

Knoll, G. F., 'Radiation Detection and Measurement', *John Wiley and Sons, Inc.*, New York, NY, 1979.

Levine, G. L., 'Characterization of the RAL and HUGINS Imaging Electron Spectrometers', *Master's Thesis*, 1994.

Peredo, M., *et al.*, 'Polar Orbit', http://www-spof.gsfc.nasa.gov/orbits/menu_orbits.html, 1996.

Perry, C.H., 'RAL CEPPAD IES Simulation Software, v0.2.1 Alpha, Users Guide', 1996.

Sullivan, J.D., 'Geometrical Factor and Directional Response of Single and Multi-Element Particle Telescopes', *Nuclear Instruments and Methods*, **95:** 5-11, 1971.

Wilken, B., *et al.*, 'RAPID, The Imaging Energetic Particle Spectrometer on Cluster', *Space Sci. Rev.*, **79:** 399-473, 1997. Also reprinted in 'The Cluster and Phoenix Missions', edited by Escoubet, C. P., *et al.*, *Kluwer Academic Publishers*, Dordrecht/ Boston/London, 1997.

Young, A., *et al.*, 'Boston University Space Acquisition Center', http://buspace.bu.edu/BUSPACE/BUSPACE.html, 1996.